Open access • Journal Article • DOI:10.2514/1.J060211

Investigation of Blowing and Suction for Turbulent Flow Control on Airfoils

Georg Fahland, Alexander Stroh, Bettina Frohnapfel, Marco Atzori ...+3 more authors

Institutions: Karlsruhe Institute of Technology

Published on: 05 Jul 2021 - AIAA Journal (American Institute of Aeronautics and Astronautics (AIAA))

Topics: Suction

Investigation of Blowing and Suction for Turbulent Flow Control on Airfoils

Georg Fahland *, Alexander Stroh † & Bettina Frohnapfel ‡
Karlsruhe Institute of Technology (KIT), Karlsruhe, D-76131, Germany

Marco Atzori §, Ricardo Vinuesa ¶ & Philipp Schlatter ‖
Royal Institute of Technology (KTH), Stockholm, SE-100 44, Sweden

Davide Gatti **
Karlsruhe Institute of Technology (KIT), Karlsruhe, D-76131, Germany

An extensive parametric study of turbulent boundary layer control on airfoils via uniform blowing or suction is presented. The control is applied on either suction or pressure side of several 4-digit NACA-series airfoils. The considered parameter variations include angle of attack, Reynolds number, control intensity, airfoil camber and airfoil thickness. Two comprehensive metrics, designed to account for the additional energy required by the control, are introduced to evaluate the net aerodynamic performance enhancements. The study confirms previous findings for suction side boundary layer control and demonstrates the interesting potential of blowing on the pressure side under various conditions, which achieves a maximum total net drag saving of 14% within the considered parameter space. The broad parameter space covered by the presented Reynolds-average Navier-Stokes (RANS) simulations allows for more general conclusions than previous studies and can thus provide guidelines for the design of future detailed experimental or numerical studies on similar boundary layer control schemes.

Nomenclature

b	=	connection line of B and F
B	=	probe point in polar diagramm
c	=	chord length
c_d	=	drag coefficient
$c_{d,f}$	=	friction drag coefficient

*Doctoral Student, georg.fahland@kit.edu
†Senior Scientist
‡Full Professor
§Doctoral Student, atzori@mech.kth.se
¶Associate Professor
‖Full Professor
**Senior Scientist, davide.gatti@kit.edu

$c_{d,p}$	=	pressure drag coefficient
c_f	=	friction coefficient
c_l	=	lift coefficient
c_m	=	pitch moment coefficient
c_p	=	pressure coefficient
C	=	perimeter of airfoil
$C_{\omega,w}$	=	ω wall function coefficient
$d_O[m]$	=	outlet distance
E	=	aerodynamic Efficiency $E = c_l/c_d$
$f[\%\text{ of } c]$	=	airfoil camber
F	=	base point for enhancement calculation
H_{12}	=	boundary layer shape parameter
$k[m^2/s^3]$	=	turbulent kinetic energy
$p[m^2/s^2]$	=	pressure
$P[J/s]$	=	power
r	=	residual
$r_C[m]$	=	radius of inlet
Re	=	Reynolds number with airfoil chord length c and free-stream velocity U_∞
t	=	tangent in B
$t[\%\text{ of } c]$	=	thickness of airfoil
$U[m/s]$	=	velocity
$U_\infty[m/s]$	=	free-stream velocity
$v_{\text{BLC}}[\%\text{ of } U_\infty]$	=	control velocity perpendicular to wall
$\{X, Y, Z\}$	=	global rigid body coordinate system
$X_{\text{tr}}[\%\text{ of } c]$	=	tripping location
$\{x, y, z\}$	=	local wall coordinate system
y^+_{wall}	=	dimensionless distance of the center point of the first cell of a wall to this wall
$\alpha[()^\circ]$	=	angle of attack
β	=	cell height correction coefficient
β_1	=	constant of $k\omega$-SST model
γ	=	constant of $k\omega$-SST model
$\delta[m]$	=	boundary layer thickness

$\delta_\theta [m]$	=	momentum thickness
$\delta^\star [m]$	=	displacement thickness
η	=	efficiency of pump/turbine
$\nu [m^2/s]$	=	kinematic viscosity
ξ	=	quality of squareness
$\rho [kg/m^3]$	=	density
σ_ω	=	constant of $k\omega$-SST model
$\omega [1/s]$	=	specific dissipation
τ_W [Pa]	=	wall shear stress
Superscrips		
N	=	value corrected by dimensionless BLC-system power consumption
+	=	value in viscous wall units
Subscrips		
as	=	air supply/discharge
D	=	values linked to aerodynamic drag
min	=	minimal
P	=	values related to pump operations
T	=	values related to turbine operations
$\perp$	=	perpendicular

I. Introduction

Air traffic is constantly growing despite its impact on carbon dioxide emissions, prompting the development of strategies to improve aircraft efficiency. During the last decades, major savings could be achieved by optimizing engine efficiency and geometrical features like planform and winglets [1]. Despite their potential, viscous drag reduction techniques have not yet found widespread application in the aeronautic industry. A notable exception is found in the field of transition control, with strategies for transition delay being implemented in full-scale demonstrators [2] and in regular operations in the Boeing 787-9 [3], although limited to the vertical and horizontal stabilizer.

Passive control devices require no additional energy to be transferred to the boundary layer and thus no complex actuator systems for their deployment. The surface structuring known as riblets belongs to this category and showed to improve overall aircraft efficiency by $\approx 4\%$ in real-flight tests [4]. Despite this efficiency increase, the increased effort for application and maintenance of the surface structures made their application economically non-profitable. At the cost of additional energy input, active control schemes promise to achieve larger viscous drag reduction in a variety of flight

conditions and possibly net improvements of aircraft efficiency [5]. A measure with very little additional energy input is to excite the natural instability frequencies of separated airfoil flows using a pulsed jet so that a turbulent boundary layer (TBL) with strong coherent vortices develops. The scheme performance can be adjusted by changing the actuating frequency to achieve either maximum lift or maximum drag reduction [6], in which case drag savings of up to $\delta c_d = 50\%$ have been reported [7]. However, its main mechanism of preventing flow separation through momentum exchange enhancement [8] is only possible if the flow shows separation in the uncontrolled case. This limits possible drag savings to scenarios like e.g. high angle of attack or aircraft with airfoil geometry restrictions other than aerodynamics. Another interesting application is focused on low Reynolds number flows as occurring, for instance, for UAVs. Such scenario features flow separation problems for fairly low angles of attack already. Additionally, these low Reynolds numbers also allow for DNS simulations of such flow regimes as shown by Zhang [9]. Partly due to a smaller prospect of improvements and partly owing to their complexity, active strategies for viscous drag reduction of turbulent boundary layers (TBL) on wings have been less frequently implemented so far. Considering the aforementioned development of air traffic and the increasingly stringent regulations on emissions, even small improvements of aircraft efficiency can have a sizeable impact and are therefore worth consideration. An advantage of turbulent flow control compared to laminar flow control or Hybrid Laminar Flow Control (HLFC) [5] lies in its stronger robustness to errors. In fact, transition control can potentially become ineffective if transition to turbulence is forced to occur upstream of the control device by adverse conditions such as, for instance, the presence of dirt particles. Being designed for the persistent turbulent regime, turbulent flow control is not subject to this limitation.

The feasibility and effectiveness of suction in TBL to improve performance of high-lift devices was already introduced by Prandtl *et al.* in the 1920s [10]. The first theoretical and experimental investigations on friction drag reduction by blowing in TBL were reported in the 1950s [11, 12]. In the 1960s several studies were carried out regarding both cooling and drag coefficient changes by mass injection through porous plates [13, 14]. Gersten and Wiedemann showed a theoretical approach on how to apply a combination of suction and blowing to a Joukowsky airfoil in the 1980s [15]. The first numerical studies in TBL were performed in the early 1990s confirming the strongly pronounced effect of wall transpiration on the local skin friction drag [16–18]. The corresponding feasibility and potential for compressible flow was shown by Hwang [19]. In recent years the theoretical drag reduction potential of blowing for skin friction drag reduction in TBL was shown *e.g.* by Kametani *et al.* [20] or Stroh *et al.* [21] using high-fidelity simulations.
Most of the aforementioned studies on the effect of wall-normal blowing and suction consider canonical flows, for which drag portions related to viscous phenomena, *i.e.* viscous drag, and skin-friction drag coincide. While invaluable to understand the effect upon near-wall turbulence, they do not consider the global impact of the control, such as the interaction between various sources of drag relevant for aircraft, including airfoil pressure drag, the additional drag corresponding to power supply for the control system and the impact on lift-generating capabilities. Some investigations regarding these fields have been performed experimentally by Kornilov [22, 23].

The present study aims at understanding the global effect of localised blowing and suction applied at the walls of a turbulent boundary layer developing on an airfoil. A challenging aspect of such a study is the large number of involved flow and control parameters which are potentially relevant for the result of the control. These include, for instance, the choice of the airfoil shape and its angle of attack (AoA), the Reynolds number , as well as the position and intensity of the control itself. The large parameter space cannot be spanned via high-fidelity Direct Numerical Simulation (DNS) or Large-Eddy Simulation (LES), owing to their large computational costs. This limits their use for the intended parameter study on airfoils to a small parameter set of single characteristic operating points, as e.g. provided by Atzori *et al*. [24]. The potential theory applied to a boundary element method coupled with the integral method for boundary layers belongs to the other end in terms of computational costs for airfoil design and involves the largest degree of modelling. This approach is broadly used e.g. by tools such as XFOIL developed by Drela [25]. These approaches, however, are based on correlations for naturally developing boundary layers, the validity of which cannot be guaranteed a priori for the particular flow control scenarios considered in the present work, but would have to be accounted for by developing customized boundary layer formulations [5]. Midway between the two extremes, Reynolds–averaged Navier–Stokes (RANS) equations offer a compromise between the high computational costs of DNS/LES and modeling challenges inherent to the boundary element method. In the present work, RANS simulations are chosen as means to cover the large parameter space of our investigation with acceptable accuracy and relatively limited modeling effort. The correctness of the approach is verified whenever possible with the well-resolved LES data by Atzori *et al*.[24].

The global efficiency of the control is measured in terms of control-induced change of total drag, lift and net aerodynamic efficiency, accounting for the additional power required for the control activation. This allows for an assessment of airfoil performance not just in one operating point but for multiple scenarios (launch/approach *vs.* cruise, main wing *vs.* stabilizer, direct drag reduction *vs.* indirect improvements), which pose various challenges on system performance.

The manuscript is structured into five sections. In section II the numerical procedure including the utilized modelling is described. The control schemes which are applied to the airfoil are discussed in section III alongside the algorithms to describe their performance alterations compared to uncontrolled airfoil flow. Section IV reports the validation of several configuration cases comparing them to high-fidelity numerical reference data in controlled and uncontrolled states. Section V depicts the results of the study and discusses the observed trends. Section VI summarizes the obtained findings.

II. Methodology

The incompressible flow around airfoils is analysed via RANS simulations in order to assess the effect of active boundary-layer control via localised uniform blowing or suction on the global aerodynamic performance of the airfoil. The calculations are performed with the open-source computational-fluid-dynamics (CFD)-toolbox OpenFOAM [26].

In particular, the steady state, incompressible solver simpleFoam is used. The k-ω-SST model is employed as turbulence model [27].

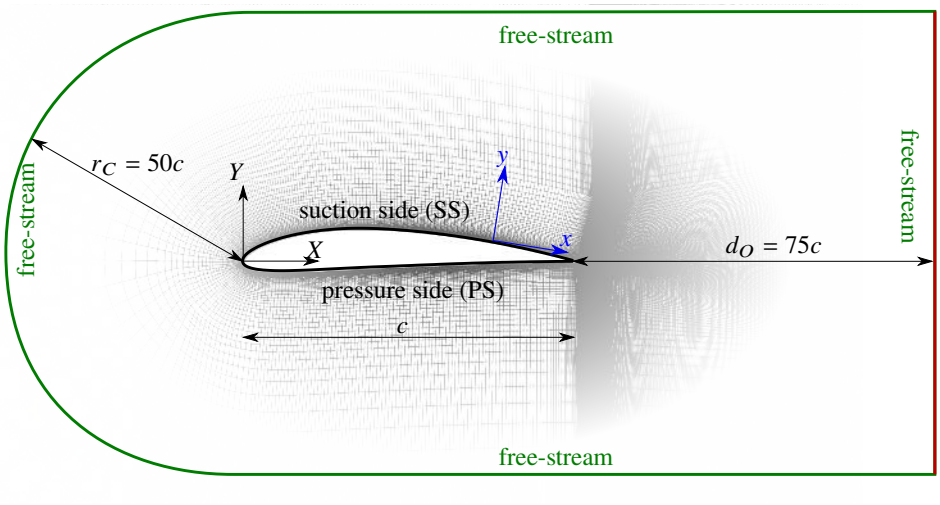

Fig. 1 Computational domain with definition of boundaries and coordinate axes: the global rigid body coordinate system $\{X, Y, Z\}$ and the local wall coordinate system $\{x, y, z\}$.

The numerical grid shown in Fig. 1 utilizes hexahedral cells in a 2D C-shaped block pattern with a C-radius of $r_C = 50c$, where c is the chord length and a trailing-edge to outlet distance of $d_O = 75c$. Meshes are generated separately for each airfoil and Reynolds number with an automated script leveraging the meshing tool blockMesh. A precursor XFOIL-calculation is executed to determine the distribution of the wall shear stress τ_w along the perimeter C of the airfoil, which determines the wall-normal mesh resolution $y_{\min}$ required for application of the turbulence model without wall functions, according to the criterion $y^+_{\text{wall}} \leq 1$. The requirement $y^+_{\text{wall}} \leq 1$ can be recast in terms of the chord length c, the speed of the incoming flow U_∞ and the local skin-friction coefficient $c_f = 2\tau_w/\rho U_\infty^2$ as:

$$y_{\min} = \beta \min_C \left(\frac{\sqrt{2}c}{Re\sqrt{c_f}} \right), \tag{1}$$

where $Re = cU_\infty/\nu$ is the chord-based Reynolds number, $\beta = 1.5$ is a coefficient to include a margin for varying angles of attack and control schemes as well as y^+_{wall} being determined in the center of the first cell whereas $y_{\min}$ describes the wall-normal height of the first cell-layer. The fullfillment of the mesh requirements for the control cases has been verified a posteriori based on the output of the RANS calculations. For the validation case (uncontrolled, NACA 4412, $Re = 4 \cdot 10^5$, $\alpha = 5°$), the maximum and average values of y^+_{wall} are 0.72 and 0.27 respectively, accommodating a margin to allow simulations of different angles of attack and controlled configurations with the same mesh. A comprehensive grid convergence study was carried out focusing on a specific case (NACA 4412, $Re = 4 \cdot 10^5$, $\alpha = 6°$) as well as some operating points with other airfoils (blunt instead of sharp trailing edge variants), AoA ($\alpha = 0°$) and different Reynolds

number ($Re = 4 \cdot 10^6$). The resulting mesh parameterization was suitable for various airfoil geometries without violating skewness, non-orthogonality and aspect rations criteria and able to reproduce validation data. The approximate total cell count of a typical airfoil mesh resulting from this was $n_{\text{cell}} \approx 110.000$ for $Re = 4 \cdot 10^5$ and $n_{\text{cell}} \approx 210.000$ for $Re = 4 \cdot 10^6$ After reaching this we evenly refined the resulting meshes for 4 different cases of the baseline airfoil NACA 4412: $Re = \{4 \cdot 10^5, 4 \cdot 10^6\}$, $\alpha = \{0°, 6°\}$. The finest meshes for $Re = 4 \cdot 10^5$ had a cell count of $n_{\text{cell}} \approx 430.000$ ($Re = 4 \cdot 10^5$) and $n_{\text{cell}} \approx 830.000$ ($Re = 4 \cdot 10^6$). Taking the results of the finest meshes as comparison the chosen parameterization stayed within an error margin of 0.6% for the airfoil efficiency E. Larger errors have been considered elsewhere as acceptable for a parameter study, *e.g.* by Kim *et al.*[28].

A sharp trailing edge configuration is utilized for the simulations, which corresponds to the setup of the LES reference configuration [24]. The LES serves as validation case for the mesh-independence study (see Section IV), which is performed by varying the overall resolution as well as individual directional mesh settings such as wall-normal and wall-parallel spacing around C. For the present study a total of 42 meshes was used covering different Re and airfoil geometries.

A. Boundary conditions

Table 1 shows the applied boundary conditions along with their OpenFOAM acronyms as well as the field values, if applicable. A homogeneous Neumann condition is imposed for the pressure p on the airfoil surface. The far-field boundary conditions for all quantities are set to be Dirichlet conditions at the inlet and Neumann conditions of vanishing gradient at the outlet. In this context, inlet and outlet are determined by the prescribed flow direction. This is important, since the change in AoA is realized by changing the inflow direction and thus also the faces where fluid actually enters the domain. On the airfoil surface the velocity $\mathbf{u}$ is set to zero except for the regions of boundary layer control where a uniform, wall-normal velocity component v_{BLC} is introduced. See section III for further discussions about the velocity distribution. At the wall, the turbulent kinetic energy (TKE) k is set to practically zero ($k = 10^{-16}$ as this is numerically more stable) as well.

Within the airfoil boundary layer, laminar flow upstream of the transition location is ensured by enforcing $k = 10^{-16}$ up to shortly upstream ($\Delta X = -1\%c$) of the intended tripping position, at which a source term is added to the TKE equation. The source term $S_{\text{k,a}}$ is treated as a semi-implicit scalar source, albeit we only use the explicit part, as described in [29]. The source term is defined in the OpenFOAM dictionary fvOptions and automatically added to the corresponding transport equation without further manual code alteration as follows [30]:

$$\frac{D}{Dt}(\rho k) = S_{\mathrm{k,a}} + H(\rho k) \quad \text{with} \quad S_{\mathrm{k,a}} = \begin{cases} 0 \frac{lunit^2}{tunit^4} \\ 2 \cdot 10^{-5} \frac{lunit^2}{tunit^4} \end{cases} \quad \mathbf{x} \in \begin{cases} X = [10\%, 11\%]c \\ y = [\delta_\theta(x, \alpha = 5°), 2\delta_\theta(x, \alpha = 5°)] \end{cases}, \tag{2}$$

where $H(\rho k)$ stands for the right-hand side of the TKE budget equation. Note that the X coordinate is given in the airfoil coordinate system whereas y is given in the wall-normal coordinate system. Also, the units apply for the incompressible formulation of the Navier-Stokes equations used in the simpleFoam solver. The intensity of the source term did not have a sizable impact on the results except for the slope of the wall shear stress transition from laminar to turbulent boundary layer.

The source term ensures an immediate transition at all considered Reynolds numbers. This setup is used to provide a realistic smooth transition from the laminar to the turbulent state, which also ensures a physical distribution of the wall-shear stress avoiding unrealistic overshooting or spatial delay. Similar transition behaviour is observed in the T3 test cases [31]. This setup is similar to the transition handling in regular transitional models like SSTγ or γ-Re_θ by Menter [32, 33] except for the prediction of the transition location. The wall-normal extension of the additional TKE source at the tripping position reaches from the local momentum thickness δ_θ to $2\delta_\theta$ and has a wall-parallel extension of $\Delta X_{tr} = 1\%c$. This includes turbulence production being initiated not directly at the wall but other than that the choice of the momentum thickness in favor of e.g. the displacement thickness as well as the height of the source resembling the exact momentum thickness is arbitrary. Yet, our validation process confirmed that this ensures an almost Re-independent tripping implementation. The application of a transitional model was found to not be feasible for the present study due to convergence difficulties and the fact that the tripping position was set to match that of the LES reference dataset in Ref. [24] and hence the chosen approach enables comparability of the configurations. For low free-stream turbulence conditions bypass transition does not typically occur and the intended tripping position is always located upstream of the free transition location, a fact that renders transition prediction within this simulation meaningless.

The specific dissipation rate ω requires a more comprehensive discussion. Owing to its definition, ω is usually assumed to tend towards infinity at the wall. Numerically, the impossibility to impose such a condition at the wall is solved through the wall function:

$$\omega = C_{\omega,w} \frac{6\nu}{\beta_1 (\Delta y)^2} \tag{3}$$

with $C_{\omega,w} = 10$. In this context β_1 refers to the equally named model constant of the $k - \omega$ part of the SST-model. The wall function of equation (3) prescribes the value of ω in the cell layer closest to the wall, while the model handles its

wall-normal propagation [27]. It must be noted that in the original k-ω-model of Wilcox [34] the function is defined with $C_{\omega,w} = 1$.

In order to account for the non-zero kinetic energy at the wall caused by wall transpiration, a different boundary condition is required, for which different proposals in the literature have been made. Wilcox [34] proposes a wall-function valid for wall blowing only, which sets the value of ω as:

$$\omega = \frac{u_\tau^2}{\nu} \frac{20}{v^+_{\mathrm{BLC}}(1 + 5v^+_{\mathrm{BLC}})} \tag{4}$$

where v^+_{BLC} is the blowing velocity. Chedevergne *et al*. [35] propose an alternative approach based on the modifications of the SST-model constants γ and σ_ω. While applicable to both blowing and suction, it relies on non-local boundary layer properties such as the local mean velocity at the edge of the boundary layer. Chedevergne *et al*. [35] verify that the difference compared to the standard SST-formulation without correction for transpiration is not significant for most applications. In the present work, we have verified that blowing cases treated with Wilcox [34] formulation (Eq. (4)) and with the standard SST formulation (Eq. (3)) exhibit differences which are at least one order of magnitude smaller than the control-induced effects.

Therefore, the boundary condition from Eq. (3) has been imposed in all cases, including those featuring wall transpiration. The marginal differences achieved through specific ω treatments combined with their additional complexity, slower convergence and model uncertainty motivate our choice to consider in the following only the standard SST formulation for ω.

variable	free-stream	airfoil surface	airfoil surface (with control)
p	*freestreamPressure* $(p_{\mathrm{ref}} = U_\infty^2)$	*zeroGradient*	*zeroGradient*
U	*freestreamVelocity* $U_\infty = \begin{pmatrix} cos\alpha & sin\alpha & 0 \end{pmatrix}^T{}_{\{X,Y,Z\}}$	*fixedValue* $(0,0,0)^T$	*fixedValue* $v_{\mathrm{BLC}}\|\|y$
k	*inletOutlet* $k = 10^{-16}U_\infty^2$	*fixedValue* $k = 10^{-16}U_\infty^2$	*fixedValue* $k = 10^{-16}U_\infty^2$
ω	*inletOutlet* $\omega_{\mathrm{in}} = 0.068\frac{U_\infty}{c}$	*omegaWallFunction*	*omegaWallFunction*

Table 1 OpenFOAM boundary conditions in their incompressible form including applicable Dirichlet values. All values are given relative to the freestream velocity U_∞ and chord length c.

B. Solution procedure

The calculations are performed by solving the incompressible RANS equations using the simpleFoam solver. In a first step, the uncontrolled solution is calculated for each mesh (hence each Reynolds number) and individual AoA with a convergence criterion requiring all normalized residuals for all field values to fall below $r \leq 10^{-5}$. These results are then used as initial fields for the parametric study. The actual simulation with boundary layer control schemes needs significantly less computational resources as the flow field already provides a similar solution for the particular AoA and Reynolds number without BLC activated. The convergence criterion for the parameter study is then set to reach $r \leq 10^{-6}$. The chosen discretization schemes are Gauss linear for gradients, Gauss linear upwind for divergence schemes and Gauss upwind for the convective schemes. All calculations are set to be steady state.

III. Control schemes and their performance

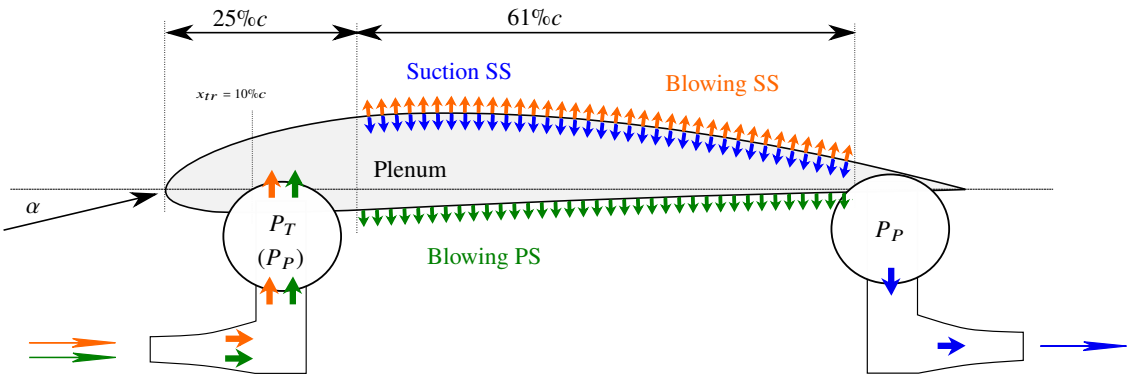

Fig. 2 Control schemes, their location and schematic of components of BLC-system which contribute additional drag (BLC-system drag).

In the following we describe the details of the considered Boundary Layer Control (BLC) schemes and introduce the metrics utilised to evaluate the control performance. The BLC considered in the present study is wall transpiration, realised as spatially homogeneous wall-normal blowing or suction. This idealisation is convenient for addressing the global effect of the control – the main goal of the present study – while avoiding to focus on the details of the large variety of possible implementations. Nevertheless, homogeneous blowing and suction do not reflect realistic implementations of the control, which necessarily involve distributed transpiration through discretely perforated plates or porous media. Since the lengthscale of e.g. a perforation is well below the resolution of the presented RANS, it cannot be directly addressed within the scope of the present modelling. However, experimental studies by Hwang *et al.*[19], at the Fukagata-Lab [36, 37] and by Kornilov [22, 23] showed that experimental implementations agree fairly well with the ideally uniform transpiration imposed numerically as far as boundary layer velocity distributions are concerned. Similar observations have been made for Laminar Flow Control through perforated plates, for which the effect of non-uniformity directly affects transition. Sizeable effort was put in minimising local disturbances, by

considering different hole patterns (*e.g.* [2, 38]), as well as in providing a suitable streamwise distribution of wall-normal velocity, e.g. by tailoring the pressure drop along the fluid supply lines for flow control [2, 39].

The region of BLC is located between $x/c = 25\%$ and $x/c = 86\%$. The general idea was to realize large but yet reasonable BLC regions regarding basic engineering hurdles: we chose the start location of $x/c = 25\%$ in order to account for an undisturbed laminar region ($x_{tr}/c = 10\%$) augmented with some downstream distance to allow for the TBL to fully develop in any operating point. The aft end of BLC was set to $x/c = 86\%$ to account for trailing edge components such as flaps, ailerons or other parts to still be implemented and furthermore ensure enough space for BLC implementation without interfering with the opposite airfoil surface. Uniform blowing is applied separately on the suction (orange plot lines) and on the pressure side (green plot lines), while uniform suction is investigated only on the suction side of the airfoil (blue plot lines), since suction on the pressure side is not expected to yield turbulent drag reduction. The color code of Fig. 2 is used throughout the entire paper to identify each control configuration.

A. Power budget

Besides modifying the airfoil lift and drag, an active BLC system impacts the overall efficiency of an airfoil configuration due to the additional power required to apply the control. For the present control strategy, additional power is required to overcome the pressure difference from the fluid supply to the controlled surface (for blowing) or from the controlled surface to the discharge (for suction) of BLC fluid, which involves pressure losses linked to the flow passing through a pipe system as well as, possibly, a porous surface or a perforated plate.

Overall, the total power P_D^N consumed by the airfoil and the BLC-system reads

$$P_D^N = P_D + P_{\text{as}} + \{P_{\text{P}} \quad | \quad P_{\text{T}}\} \tag{5}$$

with P_D being power associated to the aerodynamic drag. The power consumption related to BLC-system drag consists of two portions. P_{as} is the power consumption due to the momentum loss of the air supply at the intake or the power of the thrust resulting from the discharge of BLC-fluid. $\{P_{\text{P}} \quad | \quad P_{\text{T}}\}$ is the power to operate the pump (P_{P}) or the power which can be gained from a turbine (P_{T}) covering the pressure difference from source/sink of the BLC fluid to the supply chamber.

In order to incorporate the control input power into dimensionless aerodynamic coefficients which are usually utilised to assess the airfoil performance, the power requirements are translated in the following into effective drag coefficients. The general idea of this approach was formulated for laminar flow control by Beck *et al*. [5] and is now extended to the current setup.

The dimensionless form of the power budget in terms of drag coefficients reads:

$$c_D^N = c_D + c_{\mathrm{as}} + \{c_{\mathrm{P}} \quad | \quad c_{\mathrm{T}}\} \tag{6}$$

where we refer to c_{as} as BLC air-supply drag and to $\{c_{\mathrm{P}} \quad | \quad c_{\mathrm{T}}\}$ as pump/turbine drag.

1. BLC air-supply drag contribution

In order to provide the BLC fluid (*e.g.* air) one has to define the source (for blowing) or sink (for suction) of the fluid. Beck [5], who only considered suction cases, defines the discharge velocity at 70% of the free stream velocity, since this is the most efficient overall configuration for an assumed pump efficiency of 70%. Such a choice is not reasonable for the present study, which considers both blowing and suction, as it would over-estimate the performance of blowing configurations. This is due to the fact that the blowing case performance suffers most from the momentum loss of the air-intake at full free-stream total pressure. This momentum loss is inevitable, even in case of a passenger aircraft using exhausted cabin air as BLC fluid, since this exhaust air could otherwise be spilled in form of a jet, regaining the previously lost momentum. Therefore, discharge and supply of BLC fluid are assumed to occur at free-stream velocity. In the case of blowing, this choice means that the air-intake of the supply is at a stagnation point. For suction, the air discharge is done with a jet, which has the same total pressure as the free stream. In other words, both air supply and discharge of BLC fluid assume the internal static pressure level equal to the free-stream total pressure as seen in figure 3 indicated with the c_{as}-arrows at $c_p = 1$. The drag associated to these losses (for blowing) or gain (for suction) is regarded as air-supply-drag c_{as}:

$$c_{\mathrm{as}} = \frac{v_{\mathrm{BLC}}}{u_\infty} \frac{l_{\mathrm{BLC}}}{c}, \tag{7}$$

with l_{BLC}/c being the fraction of the BLC length per chord length.

2. Pump/Turbine power drag contribution

The second BLC-drag component c_{P} for suction BLC (or c_{T} for blowing BLC) is related to the pressure difference from the source/sink which we regard as free-stream total pressure as mentioned above and the supply chamber pressure. Figure 3 shows the graphical interpretation of BLC fluid discharge (suction, left) or supply (blowing, right). The orange rectangle shows the specific power to be provided by the pump whereas the green rectangle marks the specific power which can be gained. The green arrow represents the power related to the momentum transfer through discharge of BLC-fluid at the free stream total pressure ($c_p = 1$) while the orange arrow indicates the power related to the momentum loss by taking in fluid at the stagnation point ($c_p = 1$). Following the assumptions of Beck [5], the supply chamber pressure is assumed constant at at least $\Delta c_{p,\mathrm{loss,min}} = 0.1$ from the most unfavourable pressure value within the control region, where $c_p = 2(p - p_\infty)/\rho u_\infty^2$ is the local pressure coefficient. In Fig. 3 this specific loss is shown by the area

with black bars. Such definition automatically accounts for a velocity-square dependency of the pressure losses in the BLC piping system due to the normalization by free-stream dynamic pressure. Accordingly, only one supply chamber is needed and the uniform BLC distribution is reached by controlled losses such as fold core [39], throttle holes [2] or valves. From the energetic point of view, this is not the most favourable solution, especially if large pressure differences exist within the control region. Yet, this is a conservative estimate, which enables more realistic predictions as it incorporates the least overhead of system hardware and thus weight penalty for the aircraft.

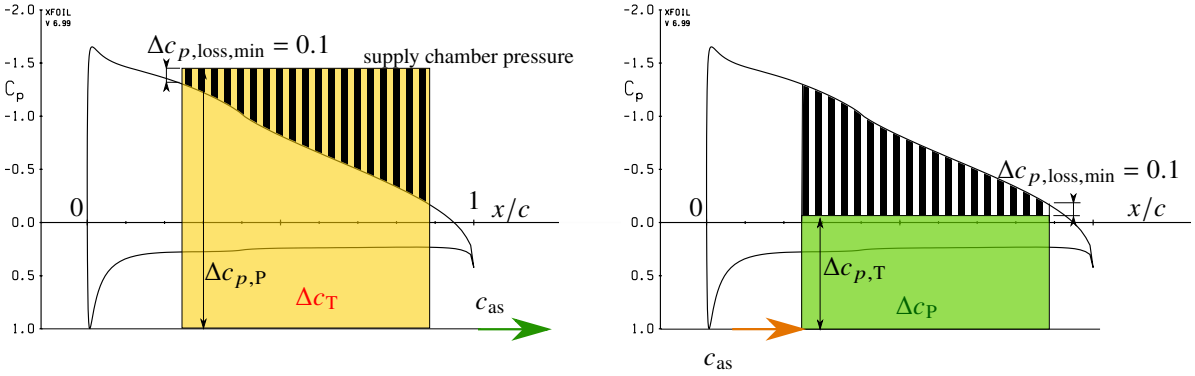

Fig. 3 Specific power consumption of BLC-system for suction on SS (left) and blowing on SS (right). Orange items account for drag, green items for drag savings/thrust.

In case of suction, further losses are caused by the pump, for which a pump efficiency of $\eta_P = 70\%$ is assumed following Beck [5]. As there is the possibility to regain energy from pressure difference in the case of blowing, a turbine can be used instead of a pump, whose efficiency is assumed to be $\eta_T = 70\%$ as well.

$$c_{\mathrm{P}} = \frac{1}{\eta_P} \frac{v_{\mathrm{BLC}}}{U_\infty} \frac{l_{\mathrm{BLC}}}{c} \Delta c_p, \tag{8}$$

$$c_{\mathrm{T}} = -\eta_T \frac{v_{\mathrm{BLC}}}{U_\infty} \frac{l_{\mathrm{BLC}}}{c} \Delta c_p. \tag{9}$$

In case of blowing c_{T} is negative whereas c_{as} is a positive drag (*i.e.* in the same direction as the airfoil drag). However, from a practical standpoint the use of a turbine might be unfavourable in terms of efficiency and additional weight. In fact, a powered aircraft has to first generate the later partially-regained BLC power by producing thrust with its engines, which exhibits a finite efficiency already. Therefore, special attention has to be paid to solutions, which offer small to vanishing turbine power as these control schemes allow for passive convection and therefore offer a notable advantage regarding overall performance.

B. Performance Enhancement

The performance of the airfoil is assessed in terms of the control-induced change of nondimensional aerodynamic coefficients, such as the lift (c_l) and drag (c_d) coefficients at various AoA, represented via the so-called polar. Performance alterations, which cannot be mimicked by a change in AoA, are the only relevant changes for the assessment of BLC. For example, at small c_l, corresponding to cruise conditions, polars exhibit a steep slope, indicating that a lift increase through BLC does not offer any benefit as a similar increase could be reached by simply increasing the AoA at the cost of marginally or even no additional drag. However, at large c_l corresponding to manoeuvre, launch and approach conditions, the polar exhibits a flatter slope, thus an increase in lift through BLC could be extremely beneficial, since a similar effect might not be achievable by increasing AoA, which is bounded by the maximum lift coefficient of the uncontrolled polar. Regarding the influence of drag on the performance, the opposite trend applies. At high c_l, a reduction of drag is not worth pursuing, especially if lift is reduced as well, whereas at the more frequent condition of low c_l, drag reduction is crucial for performance increase. This complicates the assessment of performance enhancement, which is why we define the following two metrics used throughout this study.

1. Drag reduction at equal lift

A simple metric for a given aircraft design is obtained by comparing the change in drag between a controlled and an uncontrolled polar at equal lift. This is due to the aircraft requiring a certain lift coefficient to fly at its designated cruise/launch/approach speed with a given plan-form of the air-frame. Therefore, only drag savings at the same (design) lift coefficients are relevant. Also, this metric is relevant for airfoils which usually do not generate lift (e.g. vertical stabilizer of an aircraft) but whose drag properties are relevant for the overall aircraft drag. Its mathematical representation is given in the following equation with $c_d(B)|_{\text{case}}$ being the drag of the controlled case at a given AoA and $c_d(F)|_{\text{unc.}}$ being the drag at the same lift coefficient ($c_l(F) = c_l(B)$) of the interpolated polar of uncontrolled cases:

$$\delta c_d = \left. \frac{c_d(B)|_{\text{case}}}{c_d(F)|_{\text{unc.}}} \right|_{c_l(F)=c_l(B)} \tag{10}$$

2. Perpendicular performance enhancement

A more sophisticated metric becomes necessary when comparing airfoil performance prior to defining an air-frame. In this scenario the wing plan-form and launch/approach/cruise speeds, which depend on the airfoil performance and its ability to generate lift, are still unknown. A useful metric for such scenario can be obtained by comparing two airfoil polars: the more a polar is shifted to the upper left, the higher is the performance of the airfoil, since it can generate more lift at smaller drag. Therefore, the relevant performance change is defined as the change in efficiency ratio δE between a BLC case (B) and its base point on the uncontrolled polar (F). The two points are connected by a line (b) perpendicular to the uncontrolled polar, as illustrated in Fig. 4 (right).

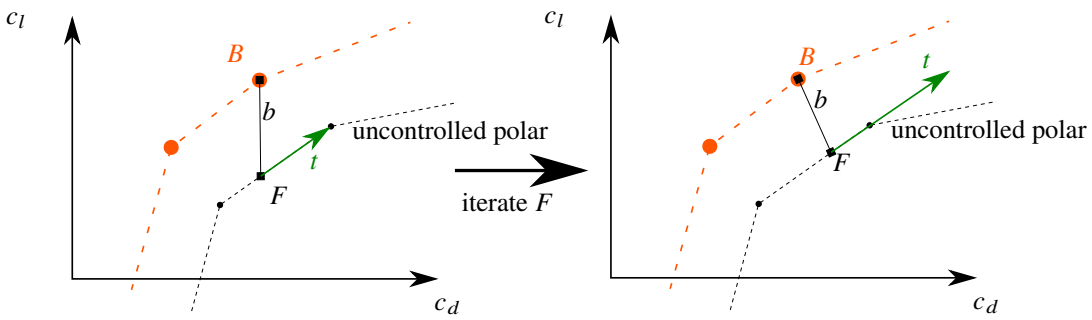

Fig. 4 Illustration of the algorithm to find the uncontrolled operating point F which to compare a controlled case B to.

Due to the different orders of magnitude of c_l and c_d, a polar plotted on equally-scaled axes is so steep that a line perpendicular to it unavoidably resembles the c_d-axis. Therefore, comparisons between the controlled and uncontrolled conditions on the polars always result in a comparison at similar c_l, which is not desirable here, as discussed above. To avoid this inconvenience, the c_d axis is rescaled by a factor which is equal to the efficiency E_F of the operating point F of the uncontrolled polar:

$$E^F = \frac{c_l^F}{c_d^F} \tag{11}$$

This is a reasonable scaling since the efficiency of an operating point F is equal to the slope of the line connecting this point to the coordinate origin. When scaling the c_d-axis with E^F the connecting line of F to the coordinate origin is the bisectrix of the c_l-c_d-quadrant. In this case we get the most meaningful visual representation of relevant performance enhancement at point F of the polar. The best possible improvement is the one which increases efficiency the most, *i.e.* an upper-left shift of the polar. In practice, we search the base point F as the projection of a given operating point B (belonging to the controlled polar) onto the uncontrolled polar. Due to the rescaling implied by equation (11) we iterate F in order to find the connecting line (b) in between B and F which is closest to perpendicular to the uncontrolled polar in the current scaling:

$$\xi = \underbrace{\frac{db^F}{dc_d}}_{\text{slope of connection line}} \cdot \underbrace{\frac{dt^F}{dc_d}}_{\text{slope of tangent in } F} = \underbrace{\frac{1}{E^F}\frac{c_l^B - c_l^F}{c_d^B - c_d^F}}_{\text{slope of connection line}} \cdot \underbrace{\frac{1}{E^F}\frac{dc_l}{dc_d}\bigg|_F}_{\text{slope of tangent in } F} \tag{12}$$

In this context ξ is a measure of how well the connecting line b represents the direction normal to t at point F. The best fit is achieved for a value of $\xi = -1$ since the slope of b and t then are the negative reciprocal of one another:

$$F = F[\min(|\xi + 1|)]. \tag{13}$$

The efficiency improvement perpendicular to the uncontrolled polar is then given as

$$\delta E_{\perp} = \frac{E^B}{E^F}, \tag{14}$$

with E^B being the efficiency of the controlled case in comparison. This approach remains fully consistent also for low c_l cases, such as symmetric airfoils at $\alpha \approx 0°$, for which also the efficiency and hence the scaling factor is small. In such cases, drag improvements are most relevant in this metric, as desired.

The advantage of this figure of merit lies in its ability to not just resolve drag savings but performance enhancement in general. For a given mission profile an increase in lift coefficient by BLC offers the possibility to reduce wing area and therefore even more total drag. This advantage cannot be evaluated by just comparing the dimensionless drag reduction at equal lift. The metrics shown in this section provide a meaningful performance assessment depending on the point of view regarding the application. The tendencies of both metrics are usually similar but of different magnitude.

IV. Comparison to well-resolved LES

In order to validate the present simulation approach the obtained results are compared against well-resolved LES data for $Re = 4 \cdot 10^5$ [40] and $Re = 2 \cdot 10^5$ [24]. In the reference database the AoA is $\alpha = 5°$ and the airfoil geometry is NACA4412 with a sharp trailing edge.

A. Aerodynamic Quantities

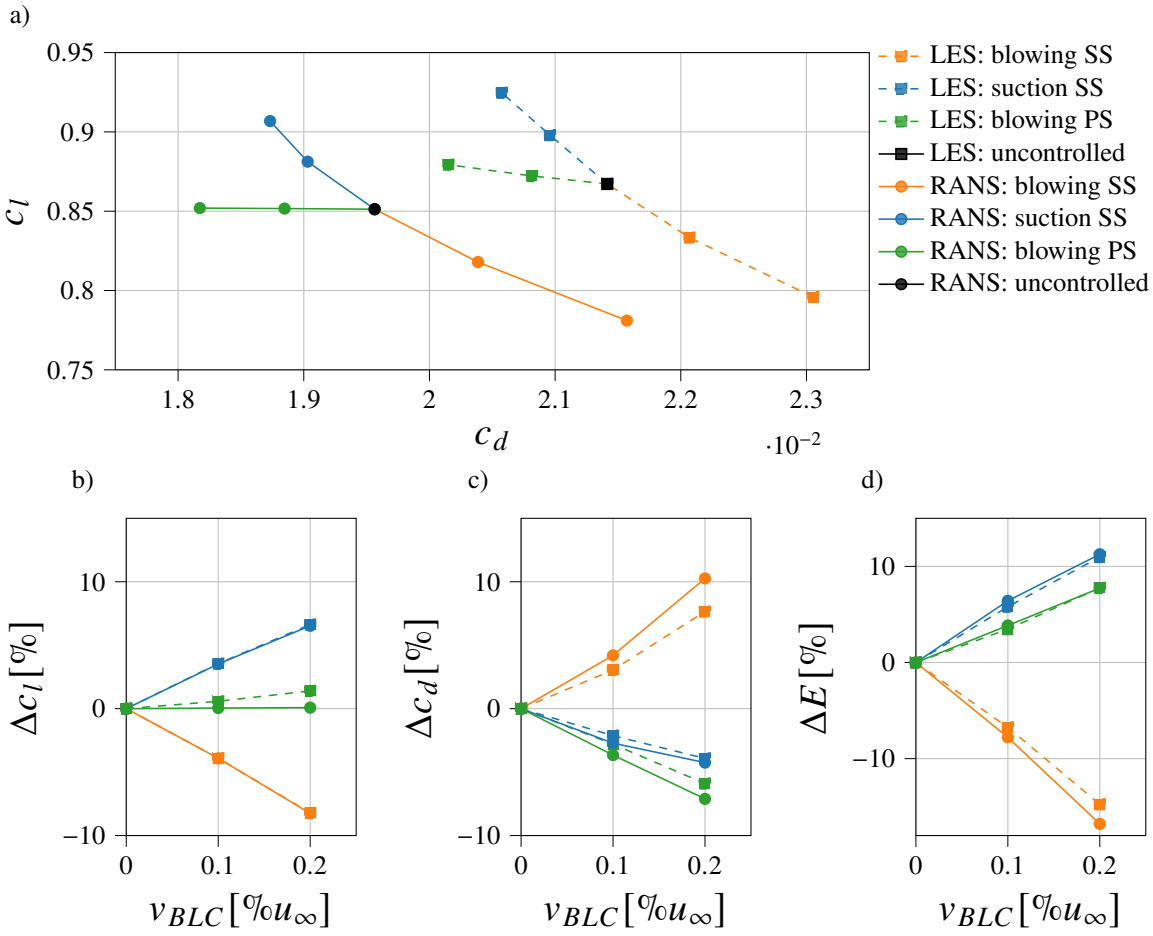

Fig. 5 Comparison of LES (dashed) and RANS (solid) predictions of the BLC effect on aerodynamic coefficients at $Re = 2 \cdot 10^5$ and $\alpha = 5°$.

The integral lift c_l and drag coefficients c_d are compared for all cases in Fig. 5(a). Figures 5(b-d) show the relative change in aerodynamic coefficients induced by the BLC with respect to the uncontrolled case for both RANS and LES simulations. Even though RANS consistently underestimates both lift ($\sim 2\%$) and drag ($\sim 9\%$) coefficients for all cases including the uncontrolled one, all trends regarding the effect of BLC are confirmed and agree reasonably well with the LES data throughout the controlled cases. A possible explanation for the differences in drag predictions is related to figure 6. As can be seen in sub-figure c) RANS predicts a smaller displacement thickness $\delta^\star$ as well as friction velocity u_τ. Note that figure 6 shows cases at $Re = 4 \cdot 10^5$ yet the effect is similar at $Re = 2 \cdot 10^5$. A smaller displacement thickness correlates with less momentum deficit in the wake and therefore smaller drag in the uncontrolled case (see also the supplemental material or [41]). The smaller friction velocity indicates reduced friction drag in the RANS compared to the LES, which is confirmed by the accumulated friction drag values for RANS ($c_{\mathrm{d,f}} = 0.011292$) and LES ($c_{\mathrm{d,f}} = 0.012764$). There are plenty of different reasons which could lead to the described effect: First of all the

applied turbulence model of the RANS does not account for curvature effects [42] which results in an error of the transport of TKE and the corresponding shear stress. It is also known that viscosity based turbulence models show problems predicting the separation points correctly [43], which in turn alters the circulation around the airfoil which feeds back on the boundary layer development. Since the circulation directly affects lift, small deviations equally affect the corresponding lift coefficient. In addition it is also possible that the different far-field domains of the presented LES and RANS are responsible for the small deviation in lift. The same is true for the tripping at $x_{tr} = 10\%$ which is realized through a source term for TKE in the RANS simulations and by a volume force term in the LES. Figure 6 a) shows that the LES produce a more sudden change in friction velocity than the RANS simulations.

There is excellent agreement in the control effects on lift (Δc_l) when the control is applied on the suction side. However, the LES results show a small lift increase when blowing is applied over the pressure side, which does not appear in RANS. Confinement effects due to the more restricted domain in the LES may be a possible explanation for this discrepancy, similar to what is observed in wind-tunnels [44], but a detailed analysis will be required to clearly identify the cause for this specific behavior. Concluding, the trends of RANS and LES align quite well for the compared cases. Since the absolute values differ, some uncertainties might remain, especially when using the RANS to extrapolate to different airfoils and Reynolds numbers. In order to rule out a systematic error regarding the general airfoil flow, comparison to various uncontrolled cases of different airfoils and Reynolds numbers was performed.

B. Localized Quantities

Figure 6(a) shows u_τ along the suction side for the validation case of $Re = 4 \cdot 10^5$, $\alpha = 5°$. The RANS simulations seem to predict consistently lower u_τ values than the corresponding LES. However, the changes induced by BLC agree surprisingly well between LES and RANS. This is true except for the flow separation predicted by RANS, which is indicated by u_τ dropping to zero whilst LES predicts no separation also with BLC in action. Interestingly, the shape factor $H_{12} = \frac{\delta^\star}{\delta_\theta}$ does not show a significant difference between LES and RANS results, despite the latter showing flow separation. RANS simulations exhibit a smaller increase of displacement $\delta^\star$ and momentum δ_θ thickness then LES once the pressure recovery reaches its steepest and constant slope (at around $x/c \approx 0.4$). This confirms previously reported findings [45, 46] that boundary layer development predictions in adverse pressure gradients have limited accuracy in eddy-viscosity based turbulence models. In this context it is important to note, that this lack in accuracy does not invalidate the predictions for flow control cases: the deviation keeps the same trends and magnitude for all three cases compared in Fig. 6.

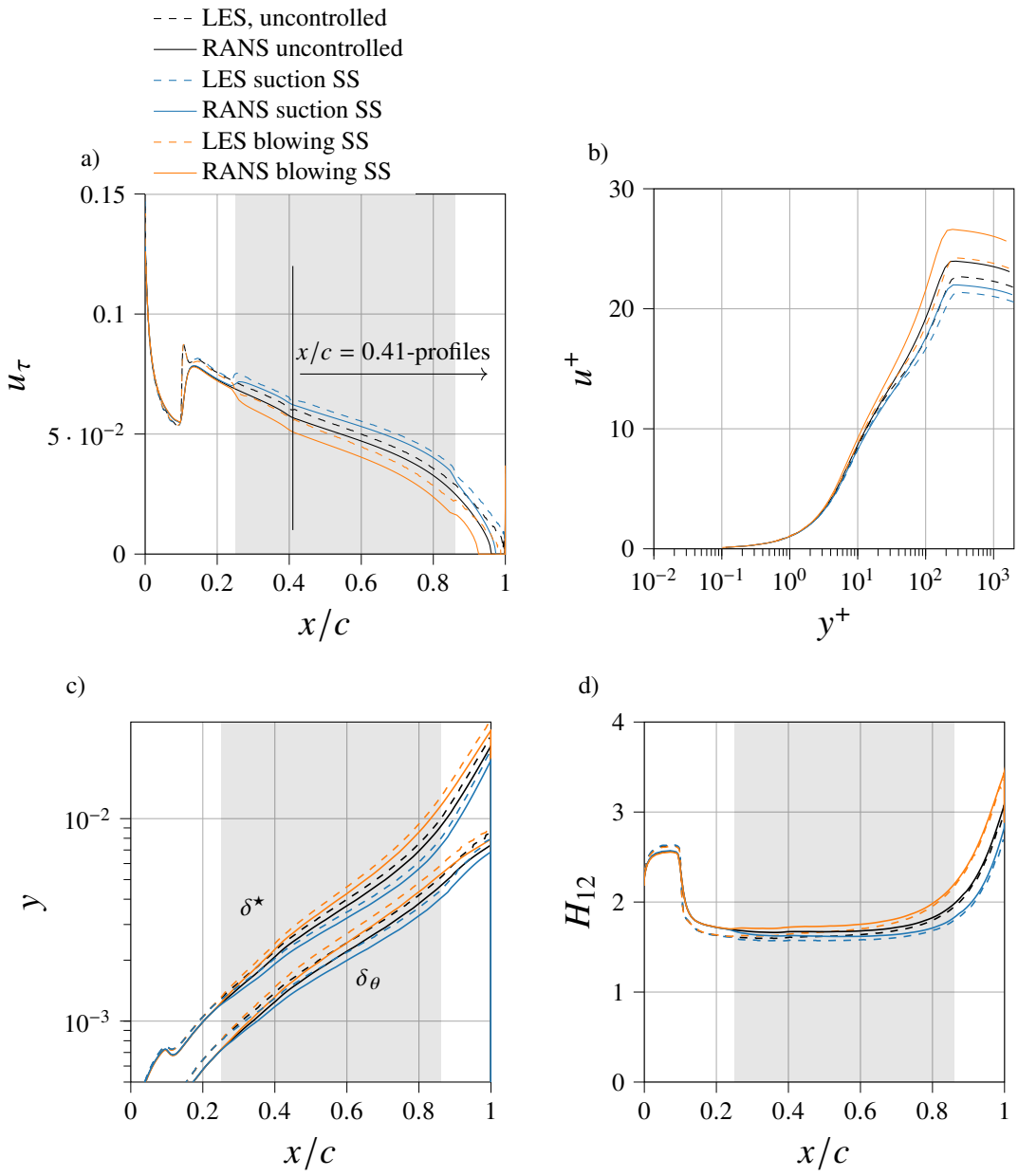

Fig. 6 Comparison of boundary-layer properties of LES and RANS. The shaded area indicates the region where BLC is active. $Re = 4 \cdot 10^5$, $\alpha = 5°$.

Figure 7 shows the comparison of LES and RANS regarding the distribution of the pressure coefficient c_p along the SS and PS of the airfoil for the validation cases. At the position $x/c \approx 2\%$ the largest deviation between pressure coefficients can be observed ($\Delta c_p \approx 0.1$ on the SS). The agreement of both setups is especially good within the BLC region which is crucial since the local changes of c_p by the BLC are only slight but still result in significant overall changes *e.g.* in lift as seen above.

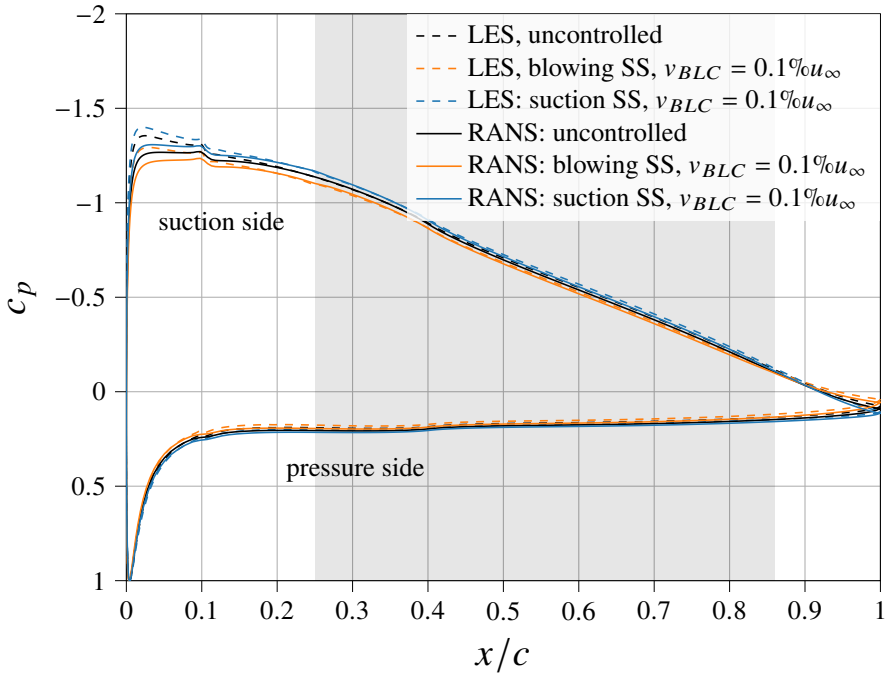

Fig. 7 Pressure coefficent c_p for $Re = 4 \cdot 10^5$, NACA 4412, $\alpha = 5°$.

V. Results

Overall a total of more than 13000 parameter combinations was investigated throughout this study. We discuss the key observations in the following. Starting with the variations of AoA (section V.A) an overview of the so-called polar plot is given since this is also the starting point for our performance evaluation. We continue with the effect of an increase in Reynolds number (section V.B) where we connect the polar plot for different Reynolds numbers to our performance evaluation metrics. The intensity variations in section V.C give a first conclusion of what control scheme seems to be most promising for further investigations. This motivates our choice to only discuss the control scheme of uniform blowing on the PS for the variations of airfoil camber and thickness in section V.D. Additional plots for more detailed informations are given in the supplemental material.

A. Effect of AoA

In this section we report the results of the parametric study with Reynolds number $Re = 4 \cdot 10^5$ and blowing intensity of $v_{\mathrm{BLC}} = 0.5\%u_\infty$ for varying values of AoA. The results are mainly analysed in terms of the polar plot presented *e.g.* in Fig. 8, which reports both the standard and effective aerodynamic coefficients, the latter accounting for the power required by the control.

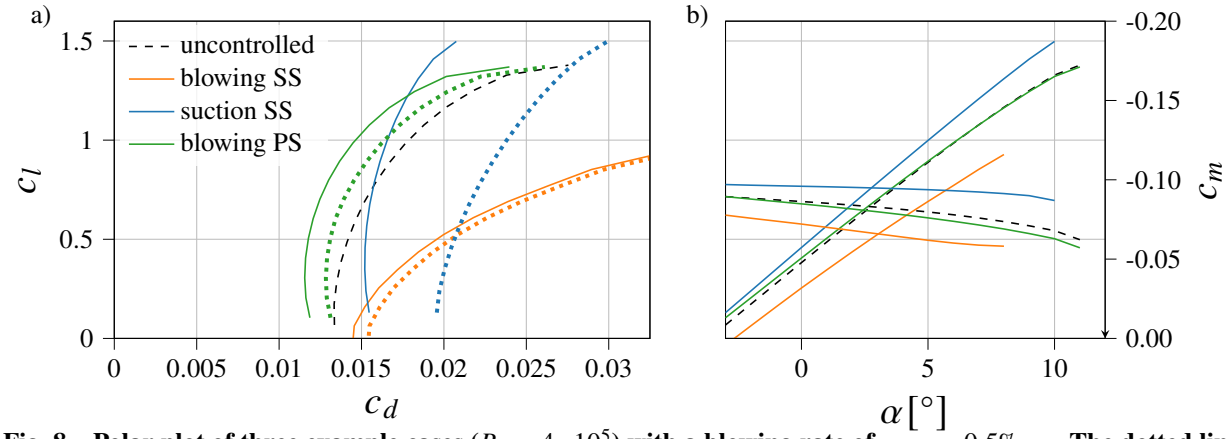

Fig. 8 Polar plot of three example cases ($Re = 4 \cdot 10^5$) with a blowing rate of $v_{\mathrm{BLC}} = 0.5\%u_\infty$. The dotted lines show the polar with an included estimate of drag associated to the BLC system.

First we discuss the effect of suction on the SS, which was already identified by Prandtl to be beneficial in high-lift configuration by preventing separation in strong adverse pressure gradient (APG) environment [10]. The effectiveness of suction on SS to enhance lift has also been demonstrated in flight by Schrenk in the 1920s [47]. The polar for suction on SS clearly shows the enhancement of c_l, which is particularly significant at larger AoA. This is also true for the increase of section moment c_m over AoA (Fig. 8(b)). The additional lift is accompanied by a reduction in drag, at least for high-lift scenarios (Fig. 8(a)). Suction increases the wall shear stress, as discussed previously [24, 48]. Thus, the drag reduction through suction on the SS is only due to the reduction of pressure drag. For small and negative AoA, *i.e.* for small enough lift coefficients, the decrease in pressure drag is entirely consumed by the increase in friction drag. As a result, suction on SS does not improve performance for low-c_l conditions, unless suction-induced relaminarisation occurs. This scenario is not considered in the present work.

With respect to blowing on SS, the aerodynamic effects are opposite to those of suction, mostly yielding an unfavorable configuration. Blowing on SS amplifies the effect of the strong APG and significantly thickens the boundary layer with respect to the uncontrolled case (see Fig. 6(c)). The resulting decrease in friction drag does not compensate for the large increase in pressure drag, as can be observed in the polar plot in Fig. 8(a). Therefore, drag is overall increased. The detrimental effect of blowing on SS is severer for stronger APG and thus for high-lift scenarios. In these situations the separation is moved upstream by BLC which can also be seen in the wall shear stress curve crossing zero at lower x-values than in the uncontrolled case (Fig. 9). In summary, BLC on the SS results in a rotation of the polar: anticlockwise (beneficial) for suction and clockwise (detrimental) for blowing.

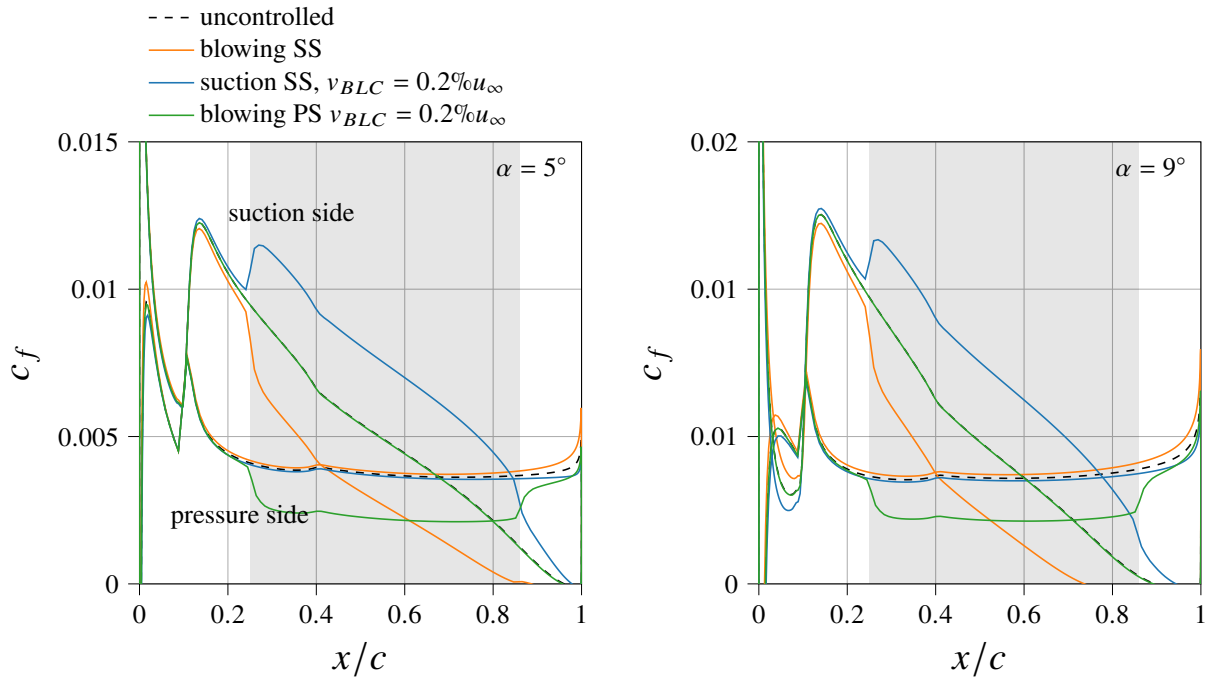

Fig. 9 Skin-friction coefficient c_f at $\alpha = 5°$ (left) and $\alpha = 9°$ (right). The shaded area represents the BLC location.

BLC on PS behaves differently due to the mild pressure gradient (*e.g.* Fig. 7). Without the interaction with a strong APG, blowing on the PS successfully reduces friction without significantly increasing the boundary layer thickness. In fact, the overall pressure drag is reduced by blowing on the PS (NACA 4412, $\alpha = 5°$, $Re = 4 \cdot 10^5$, $v_{\mathrm{BLC}} = 2\%U_\infty$: $\Delta c_{d,p} = -6.1\%$) thanks to the thrust produced by the deflection of the additional mass flux introduced by BLC towards the streamwise direction. A detailed explanation of this effect based on the integral momentum budget is provided in the supplemental material to this paper. This drag-reducing effect is always present for blowing, regardless of whether it is applied on PS or SS. However, on the SS it is exceeded by the pressure drag increase owing to the streamwise momentum deficit associated with the significant thickening of the boundary layer. Lift is essentially unaffected by blowing on the PS. Therefore, blowing on the PS yields sizeable performance enhancement, particularly at cruise conditions characterised by low-c_l values. Regarding the BLC configurations considered here, two cases are identified to improve plain aerodynamic efficiency: blowing on the pressure side and suction on the SS.

Whether the performance improvement persists after accounting for the energy required by the BLC itself is shown in Fig. 8(a) in terms of effective aerodynamic coefficients. Due to the relatively large blowing and suction rates of $v_{\mathrm{BLC}} = 0.5\%$ considered in Fig. 8, the energy consumption of the BLC fluid supply system is significant as shown by the noticeable rightward shift of the drag polar. Depending on the local value of c_p and thus on the AoA, the rightward shift depends on the profile configuration.

Figure 8(a) shows that the BLC-system induced losses for suction on SS are the largest, due to the large pressure

difference (Fig. 3) to total pressure. Conversely, blowing on the pressure side has a beneficial pressure difference which leads to the additional drag consisting of momentum loss of the BLC fluid only and no additional drag due to pump operation. Therefore, a net drag reduction is present for blowing on PS for lift coefficients up to $c_l \lessapprox 1.3$ in this particular configuration ($v_{\mathrm{BLC}} = 0.1\%$, $Re = 4 \cdot 10^5$). For suction on the SS a net increase of performance can be found for $c_l \gtrapprox 1.2$.

B. Reynolds number dependency

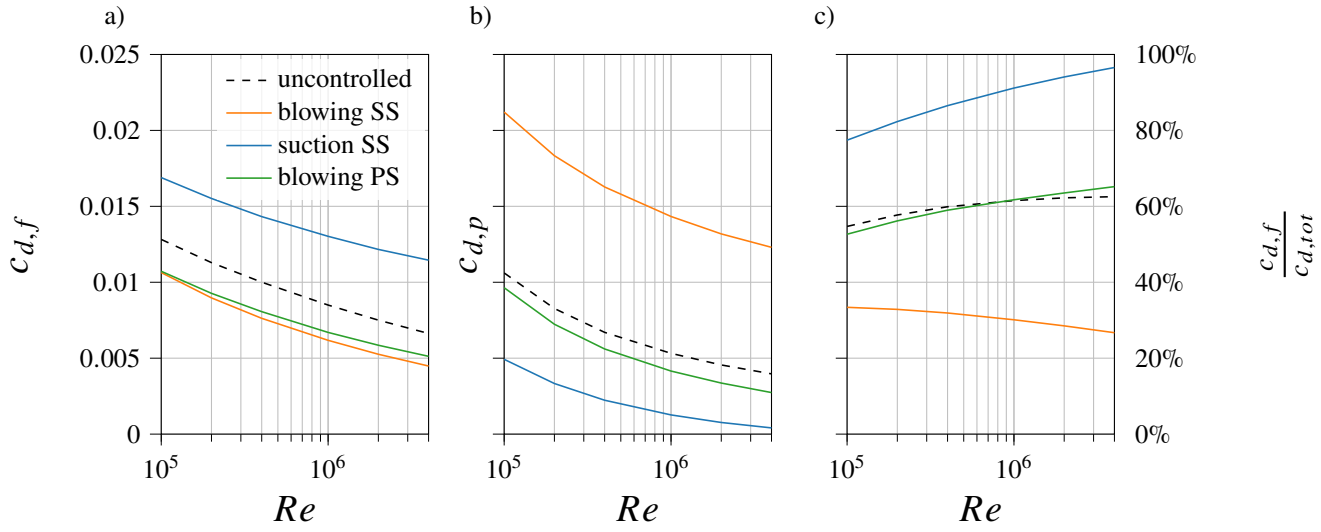

Fig. 10 Development of drag components with Reynolds number. $\alpha = 5°$, $v_{\mathrm{BLC}} = 0.5\%u_\infty$. **Friction drag** $c_{d,f}$ **(a), pressure drag** $c_{d,p}$ **(b) and ratio of friction drag to total aerodynamic drag** $c_{d,f}/c_{d,tot}$ **(c)**

In this section, the effect of the Reynolds number on the control performance is assessed by considering the configuration with AoA of $\alpha = 5°$ and the control intensity of $v_{\mathrm{BLC}} = 0.5\%u_\infty$ as baseline. Overall, as the Reynolds number increases, the lift coefficient c_l rises and the drag coefficient c_d drops. In particular, both drag contributions $c_{d,p}$ and $c_{d,f}$ decrease with Re, as it is shown in figure 10(a-c). Considering the BLC cases, the most interesting observation is that uniform blowing does not necessarily increase pressure drag despite boundary layer growth, as already discussed in the previous section.

Blowing yields similar friction drag reduction on both PS and SS, while only the former yields a reduction of pressure drag at all values of Re considered here. As a result, blowing on PS exhibits a ratio of friction-to-total drag of around 60%, which is similar to the uncontrolled case. Different results are observed for suction on SS which delivers negligible pressure drag towards $Re \rightarrow 10^7$. This means that the boundary layer is almost completely removed leaving no pressure drag at all but a solution close to the inviscid solution regarding pressure drag. The opposite is true for blowing on SS, since boundary layer growth and thus pressure drag are amplified resulting in a friction-to-total drag

ratio below 40% and exhibiting a negative slope with Re also beyond $Re = 4 \cdot 10^6$.

Figure 11. shows the development of the aerodynamic coefficients with Re leveraging the algorithm described in section III.B with all changes normalized to the values of the corresponding uncontrolled case. Further visualization of this procedure is provided in the supplemental material of this paper. The performance enhancement is evaluated either as drag reduction for equal c_l (Fig. 11(b)) or as efficiency improvement perpendicular to uncontrolled polar $\delta E_\perp$ (Fig. 11(c)). The control intensity is chosen as $v_{\mathrm{BLC}} = 0.5\%u_\infty$.

Since uniform suction reduces boundary layer thickness in a similar way as an increase of Re would do, the performance improvements relative to the uncontrolled case drop with higher Re for suction on SS. Both the aerodynamic drag reduction and efficiency improvement become negative at $Re \approx 1.3 \cdot 10^6$. Including the BLC support drag, the airfoils with suction on SS are always outperformed by the uncontrolled case at this particular AoA of $\alpha = 5^\circ$ at all Re investigated in the present study. As a result, assuming that no relaminarization occurs, suction on SS offers no direct performance enhancement within the investigated parameter space. Instead, improvements can be reached indirectly, *e.g.* by exploiting the high-lift potential through a reduction of the required wing area, especially for smaller Re at the same AoA (Fig. 11(a)).

Since uniform blowing locally increases the boundary layer thickness, the achieved variations compared to the uncontrolled case rise with increasing Re and thus overall shrinking boundary layer thickness. Blowing on SS confirms to be detrimental to performance at all considered values of Re. Although flow separation following uniform blowing is reduced for higher Re, the adverse pressure gradient on SS remains large and results in high pressure drag if blowing is applied there. Despite the rather negative effect of blowing on the SS, regarding both development with Re and AoA (previous section), the configuration may still offer possibilities related to indirect drag savings. Since the effects reported for this scheme are almost exactly opposite to the effects of suction on SS this scenario might be beneficial for roll control with the advantage of not producing a negative but positive roll-yaw moment. The combination of blowing and suction on SS could therefore replace classical ailerons similar to a solution recently adopted by BAE-Systems [49]. In principle this would lead to a possible reduction of vertical stabilizer size and its corresponding drag. The local pressure in the BLC region (Fig. 7) would also allow for passive convection thus enabling actuation via valves only.

Again, blowing on PS is the only scheme among the considered ones to consistently improve performance over the investigated parameter range. It should be noted, however, that it might be unrealistic to assume large turbulent boundary layer areas at $Re = 10^5$ on PS, as we do in the present study. However, this way the trend for the turbulent case becomes apparent and thus it is important to note that even for the highest Reynolds number investigated in this study the slope of improvement is still positive for both enhancement metrics. The same is true when the BLC support system drag is included into the effective drag coefficient. Like in the previous section, the support drag erodes roughly half of the aerodynamic improvement, with a negative trend with Re. Still, a net saving of around 14% can be reached for the blowing rate of $v_{\mathrm{BLC}} = 0.5\%u_\infty$ at the maximum $Re = 4 \cdot 10^6$ investigated here.

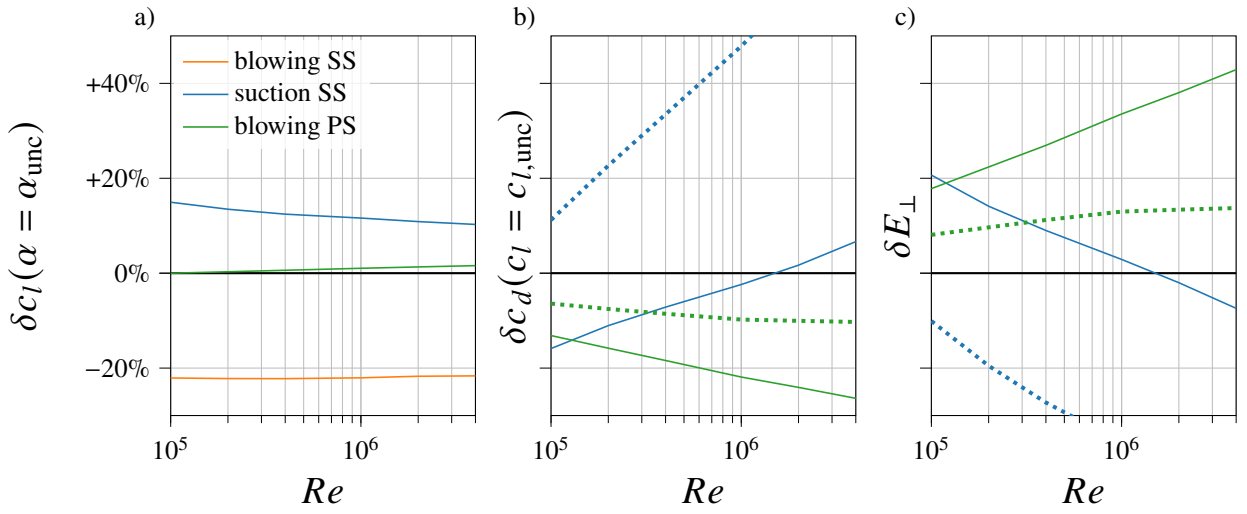

Fig. 11 Development of aerodynamic coefficients and efficiency improvement relative to the uncontrolled polar. Operating point: NACA4412, $\alpha = 5°$**,** $v_{\mathrm{BLC}} = 0.5\%U_\infty$

C. Control intensity variation

In the following, the effect of blowing and suction intensity on the control performance is addressed. An optimal intensity may result as a trade-off between maximising the control effect and minimising the energy required by the BLC. We inlcude numerous plots to the supplemental material to offer a more detailed view than our discussion can provide here. Two factors are in a conflict of interest: on one hand, intensity variation directly affects the aerodynamic properties, therefore stronger control effects are achievable at higher flow rates. On the other hand intensity defines the the BLC energy consumption, so higher intensities lead to higher consumption and reduce net energy savings. Unsurprisingly, for blowing on SS no improvement regarding efficiency can be found. In fact, the BLC polars are shifted towards the lower right of the uncontrolled polar: drag is increased and lift reduced. Moreover, the c_l-α-relation shows that progressively smaller maximum AoA could be achieved due to separation at the trailing edge, which did not allow for a steady RANS solution due to large scale vortex shedding. For $v_{\mathrm{BLC}} = 1\%u_\infty$ this already occurs at an AoA of $\alpha = 3°$, at which the corresponding lift value is decreased by almost 50% with respect to the uncontrolled case while drag is doubled. The effect of blowing on SS is quasi Re-independent.

Suction on SS shows an almost proportional increase in lift depending on the intensity v_{BLC} for a given value of α.Yet this leads to no net drag reduction except for very high c_l and low suction rates . Unfortunately, it has not been possible to quantify the maximum lift at all intensities due to convergence issues close to maximum lift conditions since this is accompanied by stronger vortex shedding which cannot be resolved with steady state RANS simulations. However, the effect of suction on maximum lift has been already discussed in literature *e.g.* [10, 47]. The development with Re is more complex than what can be observed for the blowing cases and the value of Re at which positive aerodynamic improvement vanishes depends on the blowing intensity. Nonetheless, if the support system drag is included no direct

performance improvement can be found for the given parameter set and intermediate c_l-conditions.

Blowing on PS, rather than being a rigid shift of the whole polar, results in a leftward shift of the polar which is more pronounced at intermediate lift coefficients ($c_l \approx 0.75$). This is especially true for strong blowing intensities. As a result, the benefit of blowing on PS can be exploited at best if the setup of BLC (*e.g.* its intensity) and airfoil as a whole is tailored to match the mission profile in as many operating points as possible. Similar tailoring approaches are utilised with laminar airfoils [50], which are designed in such way that the laminar bucket gets most exploited for the intended aircraft mission profile. The control-induced modification of the polar not only depends on the blowing intensity but also on the airfoil geometry, as discussed in section V.D. Therefore, it is reasonable to think that this already promising configuration can be further improved if the airfoil geometry and BLC are designed jointly. The aerodynamic performance improvements follow an almost proportional pattern with intensity and Reynolds number variation in the logarithmic scaled plot. However, the net drag and efficiency saturate with Re, since the absolute drag values go towards a saturation with rising Re while the dimensionless support drag is Re-independent. For the lower blowing intensities of $v_{\mathrm{BLC}} = [0.1, 0.2]\%u_\infty$, this saturation occurs at larger values of Re than those considered in the present study. For higher blowing rates of $v_{\mathrm{BLC}} = [0.5, 1]\%u_\infty$ the saturation can be found at around a net improvement $\delta E_\perp^N \approx +14\%$, almost independent of the blowing intensity. Yet, the intensity changes the Reynolds number at which the maximum net improvement is to be found.

D. Thickness and Camber Dependency

In the following the evaluation of the aerodynamic improvement through BLC is extended to airfoils of various cambers and thicknesses belonging to the 4-digit NACA airfoils series [51].

As known since the studies by Jackobs *et al*. [51], thicker airfoils are more capable of producing lift than thinner airfoils while allowing for higher structural strength of the wing. This comes at the cost of higher drag at low-lift cruise conditions, as nicely illustrated in figure 12, which also shows the polar plots for the most promising configuration of blowing on PS ($v_{\mathrm{BLC}} = 0.5\%u_\infty$, $Re = 4 \cdot 10^5$) at various thicknesses.

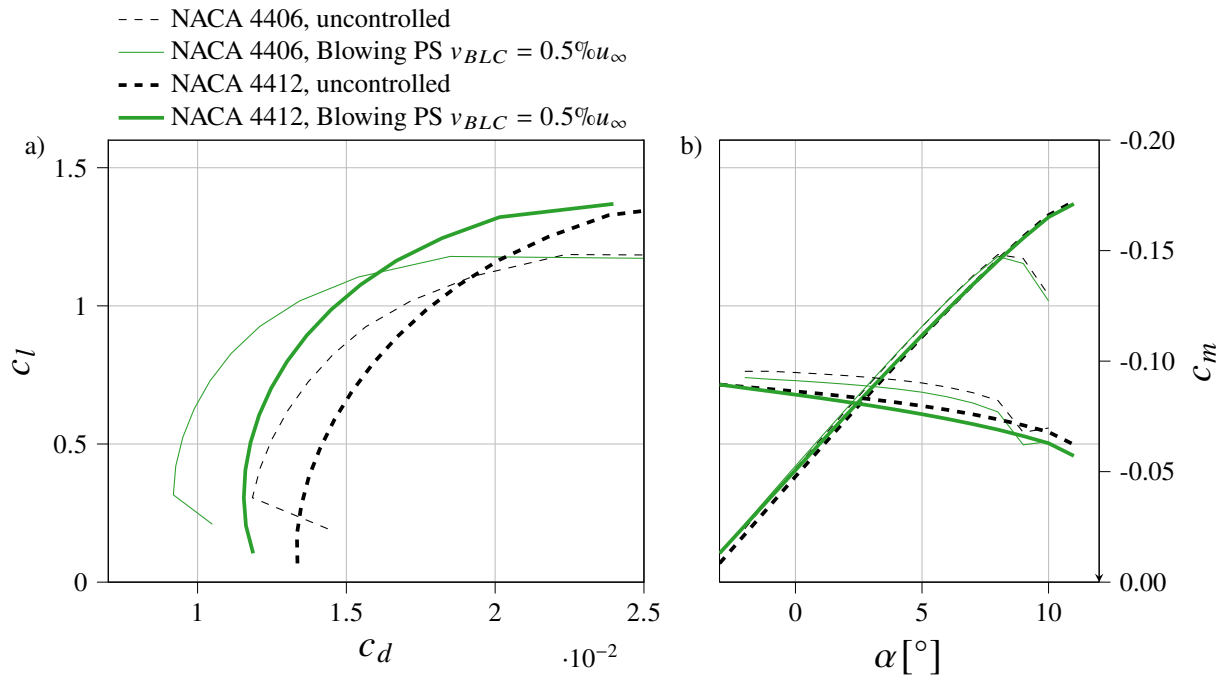

Fig. 12 Polar plot for varying thickness in case of blowing on PS with $v_{\mathrm{BLC}} = 0.5\%$. Dashed lines are uncontrolled cases

The drag reduction at low c_l is larger for thinner airfoils, while the BLC effects on c_m and c_l *vs.* AoA are minor. For the thinnest airfoil considered here (thickness $t = 6\%c$), the aerodynamic drag savings at lift coefficient $c_l \approx 0.5$ (cruise conditions, $\alpha = 2°$, $v_{\mathrm{BLC}} = 0.5\%u_\infty$) accumulate at $\delta c_d = 33\%$ for Reynolds number $Re = 4 \cdot 10^6$ and $\delta_{c_d} = 24\%$ for $Re = 4 \cdot 10^5$. Even after including the BLC system drag, a net drag reduction of respectively $\delta {c_d}^N = 14\%$ and $\delta {c_d}^N = 12\%$ is obtained.

Figure 13 shows the combined effects of simultaneously varying blowing intensity v_{BLC}, Re as well as thickness t at $Re = 4 \cdot 10^5$ at AoA of $\alpha = 5°$. Beside confirming that the BLC is more effective for thinner airfoils, it shows that the dependencies with t, Re and v_{BLC} are almost linear in the three parameters when the BLC system drag is not included into the computation. This observation might not hold for more extreme parameter variations but the scope of the study covers the most feasible variations for aviation application in incompressible flows.

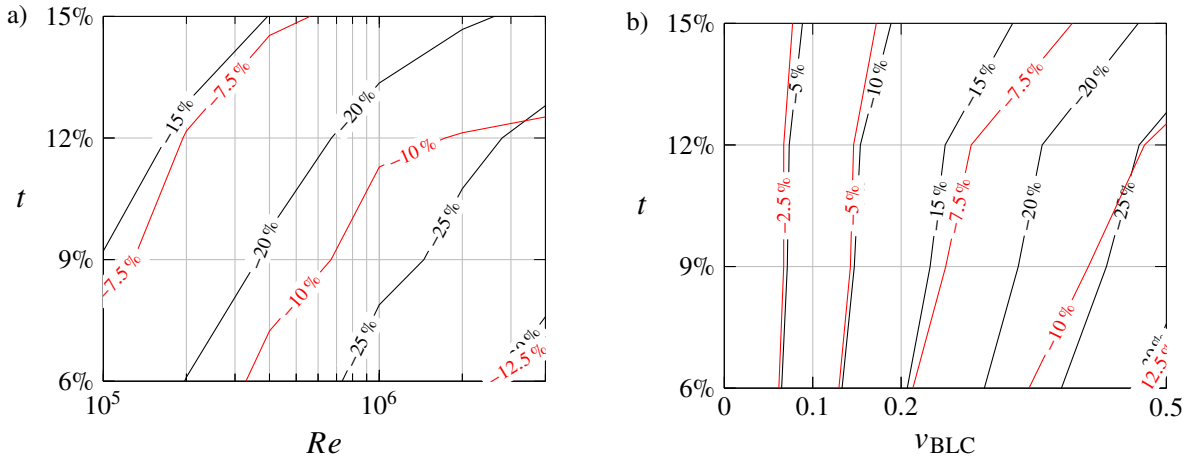

Fig. 13 Drag reduction δc_d as function of airfoil thickness t and Reynolds number Re (a) respectively blowing intensity v_{BLC} b). Plain aerodynamic comparison δc_D is plotted black, BLC-system drag included δc_D^N is plotted in red

Nonetheless, also by including BLC system drag, the Re tendency is clearly positive with a net drag reduction of $\delta {c_d}^N \gtrapprox 10\%$ for maximum $Re = 4 \cdot 10^6$ and $v_{\mathrm{BLC}} = 0.5\% u_\infty$ whereas thinner airfoils tend to yield more reduction potential relative to their uncontrolled flow.

Regarding airfoil camber we refer to the figures in the supplemental material for detailed illustration of the findings. In general, increasing camber f shifts the polar to higher c_l [51]. As long as the suction peak at the leading edge on the PS does not become too strong (see Fig. 14 for pressure distribution), substantial relative improvements can be reached for cambered airfoils at low AoAs. In principle, symmetric airfoils are more suited to be used in a low-c_l configuration, yet this is not the case including BLC: the plain aerodynamic drag at $\alpha = 0°$ is basically constant over Re and does not follow the improvement of cambered airfoils which is approximately logarithmic in Re. Including BLC supply drag, the net savings are almost totally eroded for the symmetric airfoil. This can be explained by considering Fig. 14, where the pressure coefficient on the PS of differently cambered airfoils is shown for two different AoA. Smaller camber implies a more adverse pressure gradient on the PS within the BLC region for a given AoA, a condition which intensifies at lower at AoA approaching $\alpha = 0°$. Therefore, even for high values of Re, blowing on PS acts on a turbulent boundary layer with limited capability of reducing friction drag without excessively amplifying boundary layer growth. The performance of BLC on symmetric airfoils improves for larger AoA or c_l respectively as the pressure distribution on the PS gets more favourable within the control region. Meanwhile cambered airfoils show a significant improvement over the full range of AoA investigated here.

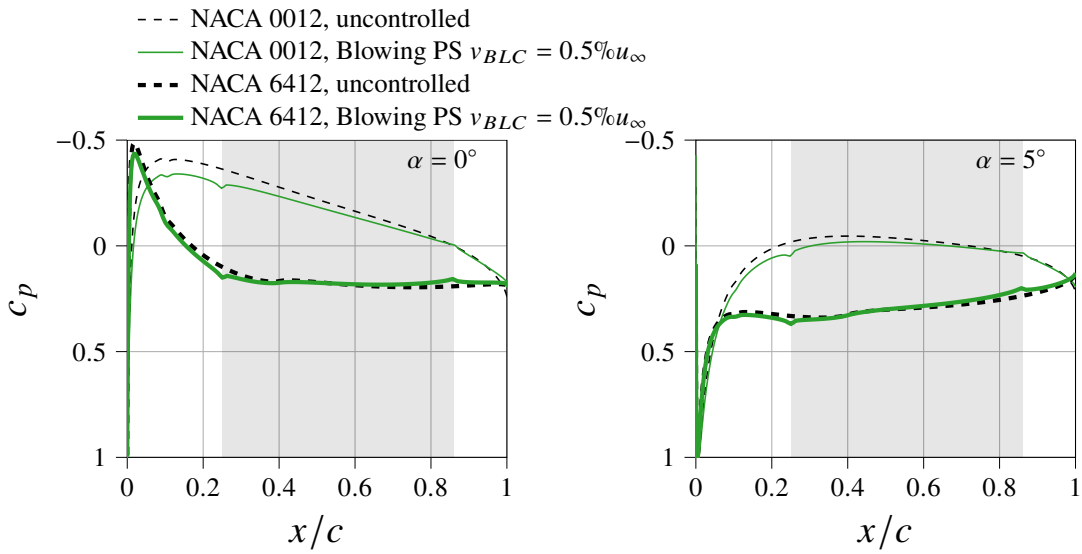

Fig. 14 Pressure coefficient c_p on PS for $\alpha = 0°$ (left) and $\alpha = 5°$ (right). $Re = 4 \cdot 10^6$. The shaded area represents the BLC location.

This finding has important implications for future research on this topic. In fact, BLC control schemes are often tested on symmetric airfoils at low-c_l conditions. This is especially true when it comes to laboratory experiments (see, *e.g.*, the combined blowing and suction on NACA 0012 [23]), large-scale show-case studies (see, *e.g.*, the HLFC on A320 vertical stabilizer [2]) or first market introduction (see, *e.g.*, the flow control on the B-787 tailplane [3]). This choice is often due to practical reasons regarding systems integration and risk reduction. The present scheme of blowing on PS shows significant net drag reduction potential, but it might not be the best choice to test it under the aforementioned zero-c_l conditions on symmetric or low-cambered airfoils. Either the scheme or the test scenario would have to be modified in order to achieve sizeable net drag reduction.

VI. Conclusion

In this paper we assess the potential performance enhancement of airfoils when localized blowing or suction is applied to the TBL developing along the airfoil. The present investigation is based on RANS simulations with fixed transition location, which are shown to yield reasonably good agreement with previous LES studies of uncontrolled and controlled flow along airfoils. The fact that RANS can reliably capture the effect of suction or blowing as BLC schemes enables the presented parameter study which provides indications about which type of suction/blowing flow control scheme has the highest potential for practical applications. The parameter study includes angle of attack $\alpha = [-3°, 12°]$, Reynolds number based on airfoil chord length $Re = [10^5, 4 \cdot 10^6]$, control intensity $v_{\mathrm{BLC}} = [0\%U_\infty, 0.5\%U_\infty]$, airfoil thickness to chord length $t = [6\%, 15\%]$ and airfoil camber to chord length $f = [0\%, 6\%]$. The control schemes investigated are uniform blowing on the SS and PS (separately) and uniform suction on the SS. These schemes are applied

in the region $X/c = [0.25, 0.86]$. In order to assess the net flow control performance, power requirements associated with the control technique are evaluated and interpreted as corrections to the classical aerodynamic performance indicators.

The control scheme that appears to be the most interesting from an energetic point of view is the one where uniform blowing is realized on the PS of the airfoil. In addition to effective drag reduction, which increases with increasing Reynolds number, this set-up also requires relatively small control power input resulting in a net drag reduction up to $\delta_{c_d}^N \approx 14\%$ for the parameter space considered here. The result that blowing on the PS can decrease pressure drag although the boundary layer is mildly thickened might seem counter-intuitive first but can be explained through the thrust generated by the deflection of the BLC mass flux. The reduction of viscous drag is thus related to an inviscid mechanism in this case. In an inviscid flow, a point source of fluid on the body surface implies a negative drag (*i.e.* a thrust). The pressure drag reduction via blowing is only visible if not outweighed by the drag-increasing effect of the additional boundary layer growth.

In contrast to blowing on the PS, blowing on the SS was not found to yield a global benefit in the investigated parameter range. This is mainly due to the fact that the achieved friction drag reduction is accompanied by a large increase in pressure drag. This increase in pressure drag is due to the adverse pressure gradient, which strongly amplifies the boundary layer growth induced by blowing. Several previous studies found that blowing on the SS increases lift in case of *e.g.* synthetic jet actuation [6–9] reduces airfoil drag, especially if separation would occur without this flow control. Yet this is not contradicted by the present study but the general effect is confirmed: in contrast to the mentioned studies, the considered uniform blowing decreases the streamwise momentum in the boundary layer and therefore acts oppositely to vortex generators or synthetic jets, which introduce additional momentum. Instead, an enhancement of near-wall streamwise momentum and therefore lift increase and drag decrease can be seen for the opposite scheme.

Suction applied on the SS of the airfoil is generally not effective at moderate lift coefficients characterising cruise flight due to a significant drag penalty. The drag increase is mostly due to the sizeable increase of friction drag associated with the thinner boundary layer. The overall effect of suction on pressure drag is mild. It results from the positive effect due to the thinner wake and the negative contribution which can be modeled as sink in potential flow theory, opposite to what was discussed for blowing. Suction (as well as control through synthetic jets) becomes interesting at high lift conditions, where it allows to achieve larger lift coefficients with lower drag than the reference configuration. However, the negative trend of the uniform suction control benefits with Reynolds number and the large energy consumption make suction in TBL regions typically not suitable for improving the aerodynamic performance, at least if it is applied permanently. On the other hand, temporary lift increases for manoeuvre, launch and approach might be an interesting application.

The broad parameter range considered in the present work delivers information about the performance of the boundary layer control schemes uniform blowing and suction in a variety of configurations. The comprehensive

information can guide the design of both future high fidelity numerical simulations and laboratory experiments. On one hand, the most promising configurations can be chosen according to the intended research goals. On the other hand, airfoil design can be performed simultaneously to the development of boundary layer control, exploiting some of the present results.

Acknowledgments

GF, DG, BF and AS acknowledge support by the state of Baden-Württemberg through bwHPC. MA, RV and PS acknowledge financial support from the Swedish Foundation for Strategic Research, project "In-Situ Big Data Analysis for Flow and Climate Simulations" (ref. number BD15-0082), from the Knut and Alice Wallenberg Foundation and from the Swedish Research Council (VR). The simulations were performed on resources provided by the Swedish National Infrastructure for Computing (SNIC) and within the project CWING on the national supercomputer Cray XC40 Hazel Hen at the High Performance Computing Center Stuttgart (HLRS).

References

[1] Lee, J. J., Lukachko, S. P., Waitz, I. A., and Schafer, A., "Historical and Future Trends in Aircraft Performance, Cost, and Emissions," Annu. Rev. Energy. Environ., Vol. 26, No. 1, 2001, pp. 167–200. https://doi.org/10.1146/annurev.energy.26.1.167.

[2] Schrauf, G. H., and von Geyr, H., "Simplified Hybrid Laminar Flow Control for the A320 Fin - Aerodynamic and System Design, First Results," AIAA Scitech 2020 Forum, American Institute of Aeronautics and Astronautics, Orlando, FL, 2020. https://doi.org/10.2514/6.2020-1536.

[3] Krishnan, K., Bertram, O., and Seibel, O., "Review of hybrid laminar flow control systems," Progress in Aerospace Sciences, Vol. 93, 2017, pp. 24–52. https://doi.org/10.1016/j.paerosci.2017.05.005.

[4] Walsh, M. J., "Riblets for aircraft skin-friction reduction," Langley Symposium on Aerodynamics, Vol. 1, 1986, pp. 557–571.

[5] Beck, N., Landa, T., Seitz, A., Boermans, L., Liu, Y., and Radespiel, R., "Drag Reduction by Laminar Flow Control," Energies, Vol. 11, No. 1, 2018, p. 252. https://doi.org/10.3390/en11010252.

[6] Feero, M. A., Lavoie, P., and Sullivan, P. E., "Influence of synthetic jet location on active control of an airfoil at low Reynolds number," Exp Fluids, Vol. 58, No. 8, 2017, p. 99. https://doi.org/10.1007/s00348-017-2387-x.

[7] Goodfellow, S. D., Yarusevych, S., and Sullivan, P. E., "Momentum Coefficient as a Parameter for Aerodynamic Flow Control with Synthetic Jets," AIAA Journal, Vol. 51, No. 3, 2013, pp. 623–631. https://doi.org/10.2514/1.J051935.

[8] Feero, M. A., Goodfellow, S. D., Lavoie, P., and Sullivan, P. E., "Flow Reattachment Using Synthetic Jet Actuation on a Low-Reynolds-Number Airfoil," AIAA Journal, Vol. 53, No. 7, 2015, pp. 2005–2014. https://doi.org/10.2514/1.J053605.

[9] Zhang, W., and Samtaney, R., "A direct numerical simulation investigation of the synthetic jet frequency effects on separation control of low-Re flow past an airfoil," Physics of Fluids, Vol. 27, No. 5, 2015, p. 055101. https://doi.org/10.1063/1.4919599.

[10] Prandtl, L., and Betz, A. (eds.), Ergebnisse der Aerodynamischen Versuchsanstalt zu Göttingen - IV. Lieferung, Göttinger Klassiker der Strömungmechanik, Vol. 7, Göttingen University Press, Göttingen, 1932. https://doi.org/10.17875/gup2009-104.

[11] Mickley, H. S., "Heat, mass, and momentum transfer for flow over a flat plate with blowing or suction," NACA, TN 3208, 1954, pp. 1–25.

[12] Black, T., Sarnecki, A., and Mair, W., The turbulent boundary layer with suction or injection, Vol. 20, ARC Cambridge, UK, Cambridge, UK, 1958.

[13] Romanenko, P. N., and Kharchenko, V. N., "The effect of transverse mass flow on heat transfer and friction drag in a turbulent flow of compressible gas along an arbitrarily shaped surface," International Journal of Heat and Mass Transfer, Vol. 6, No. 8, 1963, pp. 727–738. https://doi.org/10.1016/0017-9310(63)90043-7.

[14] Kinney, R. B., "Skin-friction drag of a constant-property turbulent boundary layer with uniform injection." AIAA Journal, Vol. 5, No. 4, 1967, pp. 624–630. https://doi.org/10.2514/3.4039.

[15] Gersten, K., and Wiedemann, J., Widerstandsverminderung umströmter Körper durch kombiniertes Ausblasen und Absaugen an der Wand, VS Verlag für Sozialwissenschaften, Wiesbaden, 1982. https://doi.org/10.1007/978-3-322-87701-7.

[16] Piomelli, U., Moin, P., and Ferziger, J., "Large eddy simulation of the flow in a transpired channel," Journal of Thermophysics and Heat Transfer, Vol. 5, No. 1, 1991, pp. 124–128. https://doi.org/10.2514/3.238.

[17] Sumitani, Y., and Kasagi, N., "Direct numerical simulation of turbulent transport with uniform wall injection and suction," AIAA Journal, Vol. 33, No. 7, 1995, pp. 1220–1228. https://doi.org/10.2514/3.12363.

[18] Park, J., and Choi, H., "Effects of uniform blowing or suction from a spanwise slot on a turbulent boundary layer flow," Physics of Fluids, Vol. 11, No. 10, 1999, pp. 3095–3105. https://doi.org/10.1063/1.870167.

[19] Hwang, D., "Review of research into the concept of the microblowing technique for turbulent skin friction reduction," Progress in Aerospace Sciences, Vol. 40, No. 8, 2004, pp. 559–575. https://doi.org/10.1016/j.paerosci.2005.01.002.

[20] Kametani, Y., and Fukagata, K., "Direct numerical simulation of spatially developing turbulent boundary layers with uniform blowing or suction," J. Fluid Mech., Vol. 681, 2011, pp. 154–172. https://doi.org/10.1017/jfm.2011.219.

[21] Stroh, A., Hasegawa, Y., Schlatter, P., and Frohnapfel, B., "Global effect of local skin friction drag reduction in spatially developing turbulent boundary layer," J. Fluid Mech., Vol. 805, 2016, pp. 303–321. https://doi.org/10.1017/jfm.2016.545.

[22] Kornilov, V. I., Kavun, I. N., and Popkov, A. N., "Modification of turbulent airfoil section flow using a combined control action," Thermophysics and Aeromechanics, Vol. 26, No. 2, 2019, p. 14.

[23] Kornilov, V., "Combined Blowing/Suction Flow Control on Low-Speed Airfoils," Flow Turbulence Combust, 2020. https://doi.org/10.1007/s10494-020-00157-7.

[24] Atzori, M., Vinuesa, R., Fahland, G., Stroh, A., Gatti, D., Frohnapfel, B., and Schlatter, P., "Aerodynamic Effects of Uniform Blowing and Suction on a NACA4412 Airfoil," Flow Turbulence Combust, 2020. https://doi.org/10.1007/s10494-020-00135-z.

[25] Drela, M., "XFOIL: An Analysis and Design System for Low Reynolds Number Airfoils," Low Reynolds Number Aerodynamics, Vol. 54, edited by C. A. Brebbia, S. A. Orszag, J. H. Seinfeld, P. Spanos, A. S. Cakmak, P. Silvester, C. S. Desai, G. Pinder, R. McCrory, S. Yip, F. A. Leckie, A. R. S. Ponter, K.-P. Holz, K.-J. Bathe, J. Connor, W. Wunderlich, J. Argyris, and T. J. Mueller, Springer Berlin Heidelberg, Berlin, Heidelberg, 1989, pp. 1–12. https://doi.org/10.1007/978-3-642-84010-4_1.

[26] Weller, H., and Jasak, H., "OpenFOAM," , 2011. URL https://openfoam.org.

[27] Menter, F., "Zonal Two Equation k-w Turbulence Models For Aerodynamic Flows," 23rd Fluid Dynamics, Plasmadynamics, and Lasers Conference, American Institute of Aeronautics and Astronautics, Orlando,FL,U.S.A., 1993. https://doi.org/10.2514/6.1993-2906.

[28] Kim, S. H., and Kim, C., "Separation control on NACA23012 using synthetic jet," Aerospace Science and Technology, Vol. 13, No. 4-5, 2009, pp. 172–182. https://doi.org/10.1016/j.ast.2008.11.001.

[29] Patankar, S. V., Numerical heat transfer and fluid flow, Series in computational methods in mechanics and thermal sciences, Hemisphere Publ. Co, New York, 1980. OCLC: 31743097.

[30] Foundation, T. O., "OpenFOAM v7 | Patch Releases," , 2019. URL https://openfoam.org/news/v7-patch/.

[31] Savill, A. M., "A Synthesis of T3 Test Cases Predictions," Numerical Simulation of Unsteady Flows and Transition to Turbulence, Cambridge University Press, 1992, pp. 404–442.

[32] Menter, F. R., Langtry, R., and Völker, S., "Transition Modelling for General Purpose CFD Codes," Flow Turbulence Combust, Vol. 77, No. 1-4, 2006, pp. 277–303. https://doi.org/10.1007/s10494-006-9047-1.

[33] Menter, F. R., Smirnov, P. E., Liu, T., and Avancha, R., "A One-Equation Local Correlation-Based Transition Model," Flow Turbulence Combust, Vol. 95, No. 4, 2015, pp. 583–619. https://doi.org/10.1007/s10494-015-9622-4.

[34] Wilcox, D. C., "Reassessment of the scale-determining equation for advanced turbulence models," AIAA Journal, Vol. 26, No. 11, 1988, pp. 1299–1310. https://doi.org/10.2514/3.10041.

[35] Chedevergne, F., and Marchenay, Y., "Transpired turbulent boundary layers: a general strategy for RANS turbulence models," Journal of Turbulence, Vol. 20, No. 11-12, 2019, pp. 681–696. https://doi.org/10.1080/14685248.2019.1702198.

[36] Hirokawa, S., Ohashi, M., Eto, K., Fukagata, K., and Tokugawa, N., "Turbulent Friction Drag Reduction on Clark-Y Airfoil by Passive Uniform Blowing," AIAA Journal, 2020, pp. 1–3. https://doi.org/10.2514/1.J059627.

[37] Eto, K., Kondo, Y., Fukagata, K., and Tokugawa, N., "Friction Drag Reduction on a Clark-Y Airfoil Using Uniform Blowing," 2018 Flow Control Conference, American Institute of Aeronautics and Astronautics, Atlanta, Georgia, 2018. https://doi.org/10.2514/6.2018-3374.

[38] Young, T., Humphreys, B., and Fielding, J., "Investigation of hybrid laminar flow control (HLFC) surfaces," Aircraft Design, Vol. 4, No. 2-3, 2001, pp. 127–146. https://doi.org/10.1016/S1369-8869(01)00010-6.

[39] Scholz, P., "Simulation of Pressure Losses for the Design of Tailored Suction Distributions for Laminar Flow Control," EDRFCM 2015, Cambridge, UK, 2015.

[40] Vinuesa, R., Negi, P., Atzori, M., Hanifi, A., Henningson, D., and Schlatter, P., "Turbulent boundary layers around wing sections up to Re_{c} = 1 , 000 , 000," International Journal of Heat and Fluid Flow, Vol. 72, 2018, pp. 86–99. https://doi.org/10.1016/j.ijheatfluidflow.2018.04.017.

[41] Althaus, D., Niedriggeschwindigkeitsprofile: Profilentwicklungen und Polarenmessungen im Laminarwindkanal des Instituts für Aerodynamik und Gasdynamik der Universität Stuttgart, Vieweg, Braunschweig, 1996. OCLC: 845149238.

[42] Hellsten, A., "Some improvements in Menter's k-omega SST turbulence model," 29th AIAA, Fluid Dynamics Conference, American Institute of Aeronautics and Astronautics, Albuquerque,NM,U.S.A., 1998. https://doi.org/10.2514/6.1998-2554.

[43] Rumsey, C. L., and Nishino, T., "Numerical study comparing RANS and LES approaches on a circulation control airfoil," International Journal of Heat and Fluid Flow, Vol. 32, No. 5, 2011, pp. 847–864. https://doi.org/10.1016/j.ijheatfluidflow.2011.06.011.

[44] Ewald, B. F. R. (ed.), Wind tunnel wall correction - La correction des effets de paroi en soufflerie, No. 336 in AGARDograph, AGARD, Neuilly sur Seine, 1998.

[45] Menter, F. R., "Performance of popular turbulence model for attached and separated adverse pressure gradient flows," AIAA Journal, Vol. 30, No. 8, 1992, pp. 2066–2072. https://doi.org/10.2514/3.11180.

[46] Yorke, C., and Coleman, G., "Assessment of common turbulence models for an idealised adverse pressure gradient flow," European Journal of Mechanics - B/Fluids, Vol. 23, No. 2, 2004, pp. 319–337. https://doi.org/10.1016/j.euromechflu.2003.07.002.

[47] Schrenk, O., "Tragflügel mit Grenzschichtabsaugung," Vol. 2, No. 1, 1928, pp. 49–62.

[48] Stroh, A., "Reactive Control of Turbulent Wall-Bounded Flows for Skin Friction Drag Reduction," Dissertation, Karlsruhe Institute of Technology, Karlsruhe, 2016.

[49] Warsop, C., and Crowther, W., "NATO AVT-239 Task Group: Flight Demonstration of Fluidic Flight Controls on the MAGMA Subscale Demonstrator Aircraft," AIAA Scitech 2019 Forum, American Institute of Aeronautics and Astronautics, San Diego, California, 2019. https://doi.org/10.2514/6.2019-0282.

[50] van Dam, C. P., "Natural Laminar Flow Airfoil Design Considerations for Winglets on Low-Speed Airplanes," Contractor Report 3853, NASA, 1984.

[51] Jackobs, E. N., Ward, K. E., and Pinkerton, R. M., "The characteristics of 78 related airfoil sections from tests in the variable-density wind tunnel," Tech. Rep. 460, NACA, Washington D.C., 1935.